2011

Modeling Groundwater Flow in Karst Aquifers: An Evaluation of MODFLOW-CFP at the Laboratory and Sub-Regional Scales

Josue Jacob Gallegos

THE FLORIDA STATE UNIVERSITY

COLLEGE OF ARTS AND SCIENCES

MODELING GROUNDWATER FLOW IN KARST AQUIFERS: AN EVALUATION OF MODFLOW-CFP AT THE LABORATORY AND SUB-REGIONAL SCALES.

By

JOSUE JACOB GALLEGOS

A Thesis submitted to the
Department of Earth, Ocean and Atmospheric Science
in partial fulfillment of the
requirements for the degree of
Master of Science

Degree Awarded:
Spring Semester, 2011

The members of the committee approve the Thesis of Josue Jacob Gallegos defended on March 18, 2011.

Bill X. Hu
Professor Directing Thesis

Ming Ye
Committee Member

Stephen Kish
Committee Member

Approved:

Lynn Dudley, Chair, Department of Earth, Ocean and Atmospheric Sciences

Joseph Travis, Dean, College of Arts and Sciences

The Graduate School has verified and approved the above-named committee members.

I dedicate this work to my Wife, Jessica.

ACKNOWLEDGEMENTS

I would like to thank God, for without his Grace, I would not have finished this work. I thank my Wife, for her patience, love, critical thinking, and extremely tasty cooking, all of which got me through the horrible days of calibrating my model. Jess, without your support I don't know what I would have done. I thank Dr. Bill Hu for taking me as his student and providing me with my first lessons on how to mathematically model, and giving me this thesis topic. A large thank you goes out to Hal Davis of the USGS, who for some reason agreed to be on my committee even though he didn't have to be. Hal took me under his wing and taught me the practical nuts and bolts of modeling, and endured many panicked and confused calls from me as I struggled to get my model to work. Thanks Hal for the tremendous amount of help. I would like to also thank Dr. Ming Ye for teaching me MODFLOW, and Dr. Stephen Kish for helping me with the geology of Wakulla Spring. Finally, but not at all least, I would like to thank Eve Kuniansky and Barclay Shoemaker of the USGS who also decided to help me with my thesis. Eve, thank you for answering all my CFP questions and looking over my CFP model. Barclay, thank you for taking the time to work on the CFP code, so that my model could run.

TABLE OF CONTENTS

LIST OF TABLES

LIST OF FIGURES

ABSTRACT

A karst aquifer is a carbonate aquifer where groundwater flow dominantly occurs through bedding planes, fractures, conduits, and caves created by and/or enlarged by dissolution. Conventional groundwater modeling methods assume that groundwater flow can be described by Darcian principles where primary porosity (i.e. matrix porosity) and laminar flow are dominant in the aquifer. However, in karst aquifers this assumption is inapplicable due to the dual porosity present in karst aquifers. While Darcian principles may apply to the matrix portion of the karst aquifer, they often do not apply to flow through conduits, where flow velocities can be great enough to invalidate the applicability of Darcy's Law. Thus, different methodologies must be used to model groundwater flow in karst aquifers. MODFLOW-CFP is a relatively new modeling program which accounts for turbulent and laminar flow in pipe like karst caves. In this study the methodology of MODFLOW-CFP is compared to several other methods to evaluate the accuracy that CFP can achieve when modeling flow in karst conditions at a laboratory and sub-regional scale. This study also briefly evaluates the program MT3DMS, to test its abilities for modeling contaminant transport in a karst aquifer analog at a laboratory scale. Results at the laboratory scale indicate that CFP is more accurate when compared to simulated results generated by MODFLOW 2005, and performs better when compared to a Navier-Stokes finite element model developed by Hua (2009). At the sub-regional scale, CFP is less accurate than the traditional MODFLOW-2000 model when comparing peak flow conditions for a simulated storm event. However, for total simulated flow for the storm event, CFP produces more accurate results than MODFLOW-2000. Regarding transport, MT3DMS can adequately simulate transport within karst at a laboratory scale.

CHAPTER ONE

INTRODUCTION

Many groundwater models are developed based on the assumption that Darcy's Law governs groundwater flow. In general this is true for groundwater flow in many aquifers. Yet under certain conditions, Darcy's Law either does not strictly apply or can be completely inapplicable. A perfect example of this is groundwater flow in karst aquifers. Due to the dual porosity of karst aquifers, turbulent flow can often occur within submerged karst features such as caves and conduits. When turbulent flow is present, Darcy's Law is inapplicable. Thus typical Darcian models often cannot accurately simulate flow in well developed karst aquifers. However, recent advances in research have yielded programs which are able to model both Darcian and non-Darcian flow within karst aquifers. MODFLOW-CFP, developed by USGS (Shoemaker et al., 2007), is such a program. MODFLOW-CFP however is a relatively new program, and little research has been done to examine the effectiveness and accuracy of MODFLOW-CFP.

The purpose of this thesis is to evaluate the ability of MODFLOW-CFP to accurately simulate flow in karst aquifers. In essence this study seeks to answer the question: will using MODFLOW-CFP (which accounts for turbulent flow, and pipe parameters) result in a more accurate model, when compared to other models that only use Darcy's Law? To answer this question, two studies were performed: a laboratory scale study and a sub-regional scale study. In the laboratory scale study, numerical models for a karst analog model were created. This study only focused on the accuracy of MODFLOW-CFP in simulating Darcian and non-Darcian laminar flow at a laboratory scale; turbulent flow was not considered for the laboratory scale study. In the sub-regional scale study, a numerical model of the Woodville Karst Plain was created. The accuracy of MODFLOW-CFP was assessed in both studies by comparing the simulated head and discharge results from MODFLOW-CFP to simulation results from Darcian models (e.g. MODFLOW-2000), as well as to actual physical.

1.1 Aquifers and Groundwater Hydraulics

1.1.1 Karst Aquifers

An aquifer is a subsurface geological formation of unconsolidated sediments or rock that is able to transmit significant volumes of groundwater. In aquifers, water is transmitted through the pores present in the rock medium. Porosity is the percentage of void space present in the rock medium. Porosity is typically divided into two categories: Primary and Secondary porosity. Primary porosity describes void space formed at the time of sediment deposition and/or lithification and is composed of intergranular void space. Secondary porosity describes void space formed after deposition due to fracturing, dissolution, or other processes (Fetter, 2001). Permeability is the ability of a rock to transmit a fluid through pore spaces within the medium (Ford & Williams, 2007). In essence, it is a measure of the interconnectedness of the void space within a rock and consequently a measure of a medium's capacity to transport water. Aquifers with rock units that have low permeability transmit less water than aquifers with rock units that have high permeability.

The term Karst is generally defined as a terrain underlain by rocks that are highly soluble (such as limestone) with well developed secondary porosity, with the terrain exhibiting distinctive hydrology and landforms such as sink holes, sinking streams, springs, and caves (Ford & Williams, 2007). According to Huntoon (1995) a karst aquifer is specifically a:

> geologic environment containing soluble
> rocks with a permeability structure dominated by interconnected
> conduits dissolved from the host rock
> which are organized to facilitate the circulation of
> fluid in the downgradient direction wherein the permeability
> structure evolved as a consequence of dissolution
> by the fluid (Huntoon, 1995, p. 343).

In this thesis, a karst aquifer is a carbonate aquifer where groundwater flow dominantly occurs through secondary porosity such as bedding planes, fractures, conduits, and caves enlarged or created by dissolution. This often results in hydrological and morphological features such as closed depressions, sinkholes, swallets/sinking streams, subterranean fractures, conduits, and caves (Figure 1).

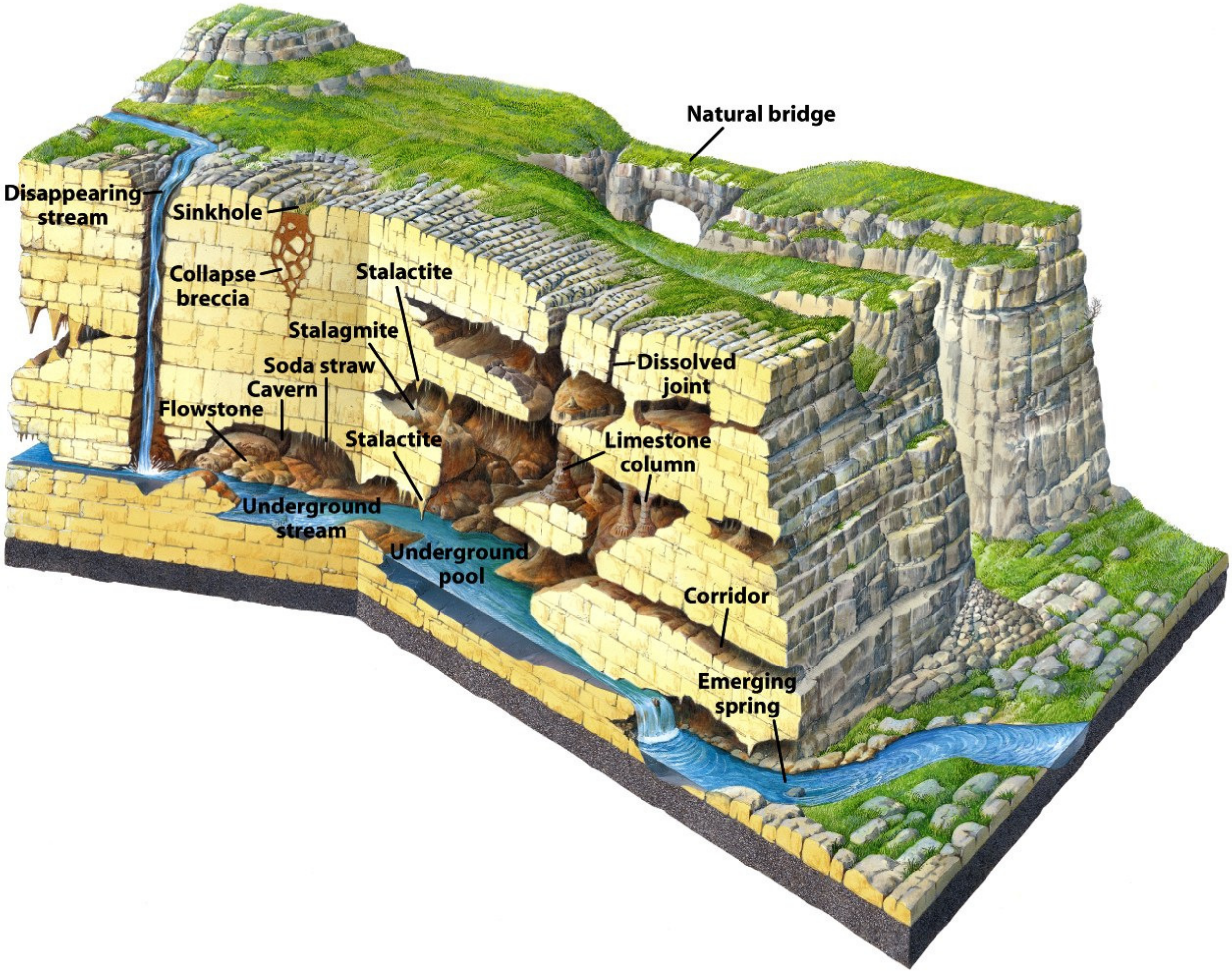

Figure 1: Karst Aquifer. This karst aquifer shows karst features such as dissolved sinkholes, caves, and fractures, through which water flows. Karst features such as caves and fractures can be partially submerged to fully submerged in water. Figure is from Marshak, 2008.

Dissolution of the bedrock to form these features is caused primarily by acidic fluids. Epigenic karst occurs when dissolution features have been formed by the movement of acidic water that infiltrated from the surface. For epigenic karst, carbonic acid is the common dissolving agent, forming when infiltrating surface water interacts with atmospheric carbon dioxide (CO_2). Hypogenic karst occurs when dissolution features have been formed by the upwelling and movement of acidic fluids from deep in the subsurface. In the case of hypogenic karst, the primary dissolving agents are hydrosulfuric acid and carbonic acid that formed from redox reactions or igneous activity (Palmer, 1991). This study will focus only on groundwater flow through epigenic karst features.

If we consider a simple case of karst development in a limestone aquifer, the formation of a karst conduit by dissolution can be divided into two phases: an initiation phase and an enlargement phase (White 1988). In both phases two dissolution regimes are present: a regime where 1st order dissolution kinetics are present, and a second regime where 4th order dissolution kinetics are present (Berner & Morse, 1974; Plummer & Wigley, 1976; Plummer et al., 1978). These studies show that when calcium concentration in water is low (under-saturated), dissolution kinetics are 1st order, resulting in fast dissolution rates of calcite. As calcium concentrations in the water increasingly become higher and approach saturation, dissolution suddenly switches from 1st to 4th order kinetics, resulting in slow dissolution rates.

During the initiation phase of a conduit, groundwater flows through small secondary porosity features (e.g. joints, fractures, bedding plane partings) and establishes a flow path from a recharge source to a discharge point. The initial aperture of the flow path is on the order of 10 to 25 µm (White 1988, p. 287). Given the small initial aperture, only a limited amount of water can flow through the flow path. This results in the water quickly approaching saturation in dissolved $CaCO_3$, as the water travels down the flow path. Because of this, 1st order kinetics are active only near the recharge point while 4th order kinetics are dominant along the rest of the flow path, resulting in a slow widening of the aperture. Over time as the aperture is slowly widened, flow increases and a higher quantity of under saturated water can penetrate deeper and deeper along the flow path, expanding the influence of 1st order kinetics further down the flow path.

Eventually a threshold is reached, termed “breakthrough” by Dreybrodt (1990). At breakthrough, the flow path aperture has widened to about 5 to 10 mm (White, 1988, p. 287), allowing the calcium under saturated water to penetrate from the recharge source all the way to the discharge point, and the flow to transition from laminar to turbulent. As a result of the calcium under saturated water now being able to flow all along the conduit, 1st order kinetics become dominant all along the conduit, producing fast dissolution rates. At this point, the initiation phase ends and the enlargement phase begins. The conduit proceeds to widen quickly, with maximum widening rates of 0.01-0.1 cm/yr (Dreybrodt 1990; Palmer 1991). Based on this general model (White, 1977; White, 1988; Dreybodt, 1990; Palmer 1991), secondary porosity features such as conduits and caves are formed by dissolution and act as highly permeable pathways for water to flow through karst aquifers.

1.1.2 Karst Aquifer Hydraulics

The dissolution of carbonate bedrock described in the previous section often results in karst aquifers having several components of porosity. This is usually described using a triple porosity model: Matrix, Fracture, and Conduit porosity (White 1988; White 2002). Matrix porosity is composed of intergranular primary porosity in unfractured rock. Apertures of matrix porosity can range from 10 – 100µm (White, 1988, p. 154). Fracture porosity is composed of secondary porosity features such as fractures, joints, and bedding plane partings within the medium that may have been partially enlarged by dissolution. Apertures of fracture porosity can range from 10 µm – 1cm (White, 1988, p.154; White, 2002, p. 89 - 90). Conduit porosity is composed of conduits and caves, which are large secondary porosity features within the medium that have been formed by dissolution. Conduits tend to have apertures that are greater than or equal to 1 cm, while cave apertures have apertures greater than 0.5 meters (White, 1988, p.154; White, 2002, p. 90). In this study a dualistic system will be used to describe the porosity of a karst aquifer: the matrix porosity domain and the conduit porosity domain. The matrix domain is composed of matrix and fracture porosity; the conduit domain is composed of conduit and cave porosity.

Since karst aquifers have multiple types of porosity, two flow types of water can occur within karst aquifers: laminar and turbulent flow. Laminar flow occurs when viscous forces in the water are dominant, overcoming the shear stresses within the water. The result is that water flows in parallel streamlines (Figure 2a). Laminar flow commonly occurs when water velocity is low and the diameters of the void spaces within the aquifer are small. Thus, laminar flow tends to occur within the matrix domain of the karst aquifer, where void space diameters are small and water velocities are slow. Turbulent flow occurs when the shear stresses in the water are dominant over the viscous forces; this is commonly caused by high water velocities and large diameter void spaces that are well connected. When flow is turbulent, water flows along non-parallel stream lines, forming complex eddies (Figure 2b). Therefore, turbulent flow occurs within the conduit domain, where void space diameters are large, permeability is high (relative to the matrix domain), and water velocities are fast.

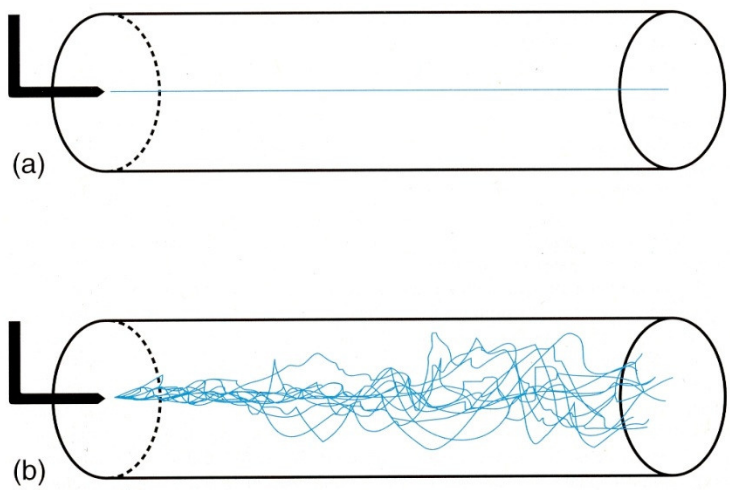

Figure 2: Laminar vs Turbulent Flow: a) dye injected into a water filled pipe, to show water streamlines when there is laminar flow, b) dye injected into a water filled pipe to show turbulent flow. Modified from Hornberger et al. (1998).

The Reynolds Number is an empirical equation that describes the laminar or turbulent flow properties of a fluid based on the fluid properties (e.g. viscosity & density). It is often used to determine whether flow is laminar or turbulent within a flow system. For a pipe, the Reynolds Number equation (Equation 1) is:

$$R = \frac{UL\rho}{\mu} \qquad \textbf{(1)}$$

where R is a dimensionless value, called the Reynolds number. U is the mean velocity, L is the pipe diameter, ρ is the fluid density, and μ is the viscosity of the fluid (Hornberger et al., 1998). Thus, equation 1 can be used to determine whether flow is laminar or turbulent in karst conduits. For smooth pipes, laminar flow occurs when R is less than 2000 (Figure 3). Turbulent flow occurs when R is greater than 4000. These two limits are commonly referred to as the Critical Reynolds numbers (N_{RE}). Between these two limits is the "transition zone" where flow is not easily characterized as laminar or turbulent. Due to this transition zone, it is common to have an upper and a lower Critical Reynolds number for pipes and conduits. The upper N_{RE} is the value above which flow becomes turbulent. The lower N_{RE} is the value below which flow becomes laminar. The lower and upper N_{RE} can change depending on how rough the walls of a conduit are.

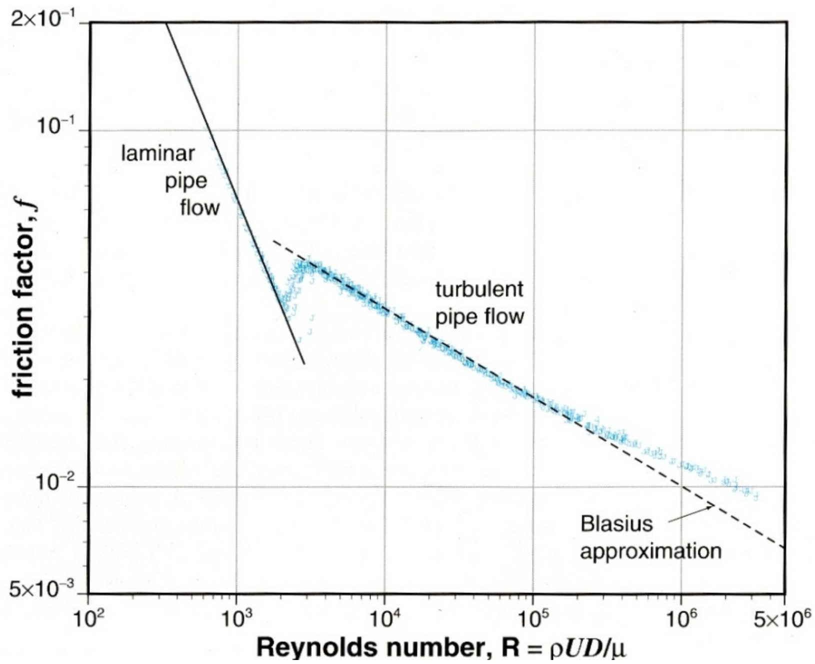

Figure 3: Friction factor vs. Reynolds number graph. This graph shows experimental results for smooth pipes. The break in measurements between R of 2000 and 4000 marks the transition zone. Modified from Hornberger et al. (1998).

With some modification, the Reynolds equation can also be applied to the matrix domain of an aquifer to determine if flow is turbulent or laminar within the matrix and fracture porosity. Instead of mean velocity, specific discharge (*q*) is used, and the conduit diameter (*L*) is replaced by the mean grain diameter (*d*) which represents the pore space (Equation 2).

$$R = \frac{qd\rho}{\mu} \qquad \textbf{(2)}$$

In general, groundwater flow is governed (or described) by Darcy's Law. Darcy's law is an empirical equation (Equation 3) obtained by Henry Darcy in 1856 from a column experiment, which describes the linear relationship of specific discharge (*q*) and hydraulic gradient (*dh/dl*), given the proportionality constant hydraulic conductivity (*K*). A common form of the equation is shown below. The negative sign indicates that flow is occurring from high head to low head.

$$q = -K \frac{dh}{dl} \qquad \textbf{(3)}$$

The limitation of Darcy's Law is that it is only applicable under laminar conditions with Reynolds numbers less than 1 to 10 (Rose, 1945a; Rose, 1945b; Hornberger et al., 1998; Fetter, 2001). These two conditions are met in the matrix of most aquifers where groundwater moves very slowly and viscous forces are dominant. However, in karst aquifers where matrix, fracture and conduit porosity are present, Reynolds numbers can often exceed the range listed above. This typically occurs in conduits within the aquifer, caused by the large diameters of the conduits and high flow velocities (White 1977; Palmer 1991; White 2002). Therefore, even though flow may still be laminar in conduits (Figure 3), the propensity for higher flow velocities and presence of large conduit diameters drives the Reynolds numbers of the conduits above 10, making Darcy's Law inapplicable within conduits.

Figure 4 illustrates a more generalized example of the validity of Darcy's law under various flow conditions. When flow is laminar with Reynolds less than N_{RE}= 1 to 10, the relationship between specific discharge and hydraulic gradient is linear, and can thus be described by Darcy's Law. As specific discharge increases and the Reynolds numbers exceed the N_{RE}, the relationship between specific discharge and hydraulic gradient becomes non-linear as flow becomes turbulent, and thus cannot be described by Darcy's Law. Thus, numerical groundwater models that use Darcy's Law are fairly accurate for single porosity media where linear laminar flow in the matrix is dominant, but can be highly inaccurate when applied to dual porosity media such as karst aquifers, where nonlinear laminar flow with R> 10 values and/or turbulent flow are common. A different approach that does not solely rely on Darcy's Law is needed to better simulate flow in karst aquifers.

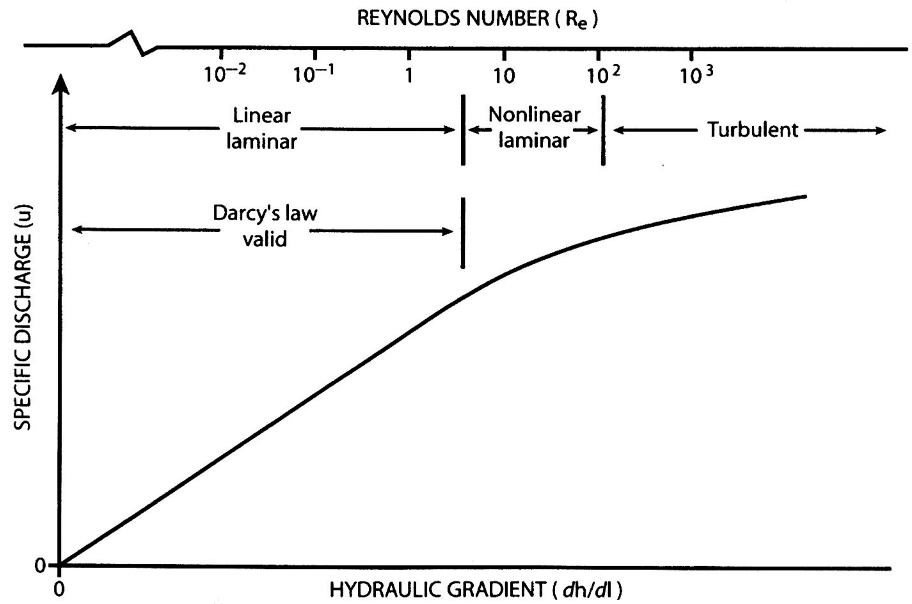

Figure 4: Hydraulic Gradient and Specific Discharge for linear laminar, nonlinear laminar and turbulent flow. Modified from Freeze & Cherry (1979).

CHAPTER TWO

LITERATURE REVIEW

Dissolution of carbonates in karst aquifers results in karst aquifers having 3 types of porosity (matrix, fracture, and conduit) which leads to laminar and turbulent flow both occurring within the aquifer. This can cause problems when attempting to numerically model groundwater flow within karst aquifers, as Darcy's Law is not always applicable. As a result, multiple methods for simulating flow in karst aquifers have been formulated and are described below.

2.1 Review of Karst Modeling & Previous Work

2.1.1 Types of Karst Models

There are multiple approaches used to simulate groundwater flow in a karst aquifer, each with its own set of advantages and disadvantages. Groundwater models can be divided into three general groups or types: Equivalent Porous Medium (EPM) models, Discrete Fracture (DF) models, and Dual Continuum (DC) models (Anderson & Woessner 2002, 329; Shoemaker et al., 2007, pg 3). EPM models (also known as single continuum or single porosity models) assume that the porous medium of a karst aquifer can be treated as a single continuum and that a representative elementary volume (REV) can be defined that accounts for both matrix and conduit porosity (Figure 5).

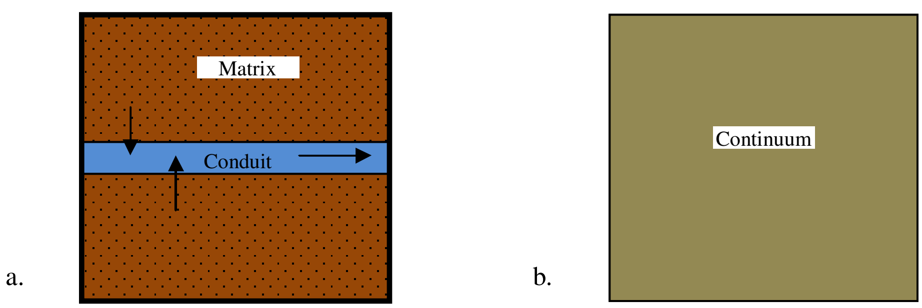

Figure 5: Equivalent Porous Medium Model Approach. a.) A simplified karst aquifer with a permeable matrix and a single water filled conduit - arrows indicate water flow direction; note that water can flow from matrix to conduit. b.) Equivalent porous medium modeling approach – this approach assumes that a single porosity continuum can represent both the matrix and conduit. porosity found in the karst aquifer.

EPM models have been successfully used to simulate flow in karst aquifers at a regional scale, and are useful when the purpose of the model is to simulate discharges, groundwater fluxes and hydraulic heads. Teutsch (1993) used a EPM model to simulate flow within an aquifer of moderate karstification near Heidenheim, in the Swabian Alb. Scanlon et al. (2003) were able to use MODFLOW to create a regional EPM model of the highly karstified Barton Springs section of the Edwards aquifer in Texas. The advantage of using an EPM model to simulate flow in karst is that prior knowledge of exact geographic location of conduits, conduit geometry and other conduit hydraulic properties (such as tortuosity, wall roughness, etc.) are not necessary to simulate flow. However, a disadvantage of using an EPM model is that they cannot simulate flow direction and flow velocity at a local scale (i.e. flow direction within specific conduits) because conduits are not explicitly represented within the model. Thus, EPM models are often not very useful for simulating transport related problems. Another related disadvantage is that EPM models assume that flow is laminar and that Darcy's Law governs flow. This may lead to water velocity and discharge not being accurately simulated since turbulent flow is not accounted for within conduits. Thus, as Huntoon (1995) noted, EPM models may be successful at the regional scale, but they can often fail to simulate karst conditions at the local scale.

DF models assume that the flow occurs primarily within the fractures or conduits, with the matrix assumed to be impermeable (Figure 6).

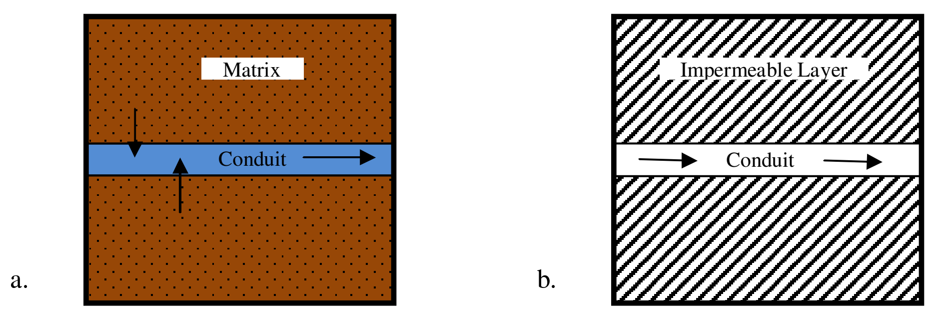

Figure 6: Discrete Fracture Model Approach. a.) A simplified karst aquifer with a permeable matrix and a single water filled conduit - arrows indicate water flow direction; note that water can flow from matrix to conduit. b.) Discrete Fracture modeling approach – this approach assumes that the matrix is impermeable and that flow only occurs along the conduit.

DF models have been used to simulate flow in theoretical and actual karst aquifers. Thrailkill (1974) simulated both laminar and turbulent flow in a Kentucky limestone aquifer. Dreybrodt (1990) used a DF model to simulate karst genesis in a theoretical karst conduit. Halihan and Wicks (1998) used a form of the DF model type to investigate the effects that conduits and turbulent flow have on a theoretical karst aquifer and its hydrograph response. Jeannin (2001) successfully simulated discharge and velocities in the Holloch cave system in Switzerland. Since flow is assumed to occur only in the conduits, hydraulic pipe equations can be used which allow DF models to simulate both laminar and turbulent flow. The distinct advantage of a DF model is that the model can simulate flow direction and water velocities within the conduits which can be used to simulate contaminant transport (Shoemaker et al., 2007, pg 3). The disadvantage of DF models is that they require data regarding location, geometry, and hydraulic properties of all the conduits, which often are unobtainable. Another disadvantage is that DF models do not account for flow exchange between the matrix and the fracture network. Thus, DF models may not simulate flow correctly in karst aquifers which have high permeability in both the conduit and matrix domains and where groundwater exchange occurs between the two domains (e.g. the Floridan Aquifer).

DC models (sometimes called double porosity models) assume that flow occurs within both the matrix porosity and fractures/conduits porosity with flow being exchanged between the two porosity domains (Figure 7).

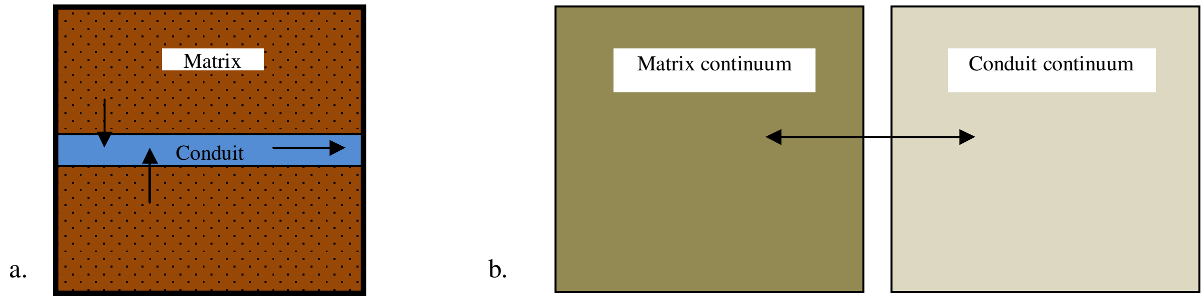

Figure 7: Dual Continuum Model Approach. a.) A simplified karst aquifer with a permeable matrix and a single water filled conduit - arrows indicate water flow direction; note that water can flow from matrix to conduit. b.) Dual Continuum approach – this approach assumes that the matrix and conduit can be represented by separate continuums.

Two continuums are used in the DC model, one for the matrix porosity, and another for the conduit porosity. The matrix continuum typically has a low hydraulic conductivity and high porosity to represent the diffuse flow that occurs within the pores and fractures of the matrix. The conduit continuum has a large hydraulic conductivity and a small porosity to represent the conduits and the high velocity flow that occurs within the conduits. A flux exchange term (which describes the rate of mass transfer between the two continuums) links the two continuums, allowing for flow to move from one continuum into the other. Teutsch (1993) successfully used a DC model to simulate flow within a highly karstified aquifer near Reutlingen in the Swabian Alb. Sauter (1993) also used a DC model to simulate flow in the Gallusquelle karst aquifer, also in the Swabian Alb. The advantage of using the DC model is that prior knowledge of the geometric parameters of the conduits within the karst is not required (Sauter, 1993). However, a large amount of hydrogeological field data is needed to calibrate a DC model. Such data is not always available and thus may limit the use of the DC model (Sauter 1993). Referencing the German studies of Teutsch & Sauter (1998) and Mohrlok (1996), Shoemaker et al. (2007) also point out that, while DC models are useful when the geometry of the conduits are unknown, DC models tend to have trouble simulating transport processes at small scales within karst aquifers.

There is a fourth type of modeling approach which is often called a coupled continuum pipe flow (CCPF) model (Figure 8).

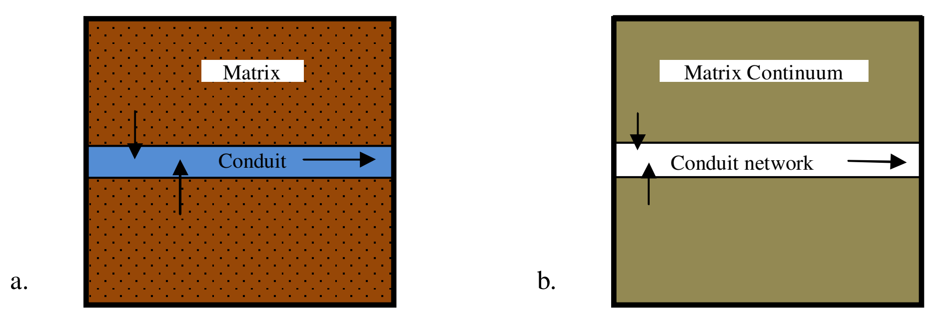

Figure 8: Coupled Continuum Pipe Flow Model Approach. a.) A simplified karst aquifer with a permeable matrix and a single water filled conduit - arrows indicate water flow direction; note that water can flow from matrix to conduit. b.) Couple Continuum Pipe Flow approach – this approach assumes that the matrix is represented by a continuum and the conduit by a discrete conduit network.

With this model type, a single continuum is coupled to a discrete conduit network. In essence, this model type is two models in one. The continuum represents the porosity of the matrix and the discrete network represents the porosity of the conduits within the karst aquifer. An exchange term accounts for flow between the continuum and the conduit network (Shoemaker et al. 2007). This model type has several major advantages when compared to the three previous model types/approaches. One advantage of the CCPF is that laminar flow in the matrix and turbulent flow in the conduits can both be simulated at the same time. Previous modeling approaches, such as the EPM model type, applied Darcy's Law to both the matrix and conduit porosities, which caused error since Darcy's Law cannot describe turbulent flow in pipes. In the CCPF model type Darcy's law is only applied to the matrix while fluid mechanic equations (e.g. Darcy-Weisbach and Colebrook-White equations) are only applied to the conduits. This allows the CCPF model to account for both laminar and turbulent flow and can result in more accurate simulations. The coupling of the conduit network also allows pipe parameters (e.g. diameters) to be input into the CCPF model, resulting in a more physically based model. Finally, with the exchange term, the water and solute exchanges between the conduit network and matrix domain can be simulated. This is important in karst aquifers such as the Floridan aquifer, where high matrix permeability results in exchange flow between the matrix and conduit porosity (Martin & Dean 2001; White 2002).

CCPF models have also been used to study groundwater flow, karst cave/conduit genesis and contaminant transport in karst aquifers. Yusun and Ji (1988) used a finite element based CCPF model to simulate groundwater flow in a synthetic karst aquifer. Clemens et al. (1996) created a CCPF model called CAVE (Carbonate Aquifer Void Evolution) to simulate conduit genesis within a karst aquifer. Bauer et al. (2003) and Liedl et al. (2003) used CAVE to conduct parameters studies investigating the effects of recharge, boundary conditions, hydraulic conductivity, and exchange coefficients on karst aquifer genesis. Spiessl et al. (2007) used CAVE and PHT3D to create a reactive transport model which can simulate transport through conduits. Shoemaker et al. (2007) also used CAVE to create a flow model called MODFLOW-CFP that simulates flow in karst aquifers that have conduits and/or vuggy porosity. Faulkner et al. (2009) used a Navier-Stokes based code by Hua (2009) to create a CCPF model of a laboratory scale karst analog flow model created by Faulkner (2008), and were able to successfully simulate head distribution and contaminant transport.

To summarize, models such as Equivalent Porous Medium (EPM) models, Discrete Fractures (DF) models, and Dual Continuum (DC) models can be used to simulate karst flow conditions. However they have some limitations. EPM models can simulate karst flow at a regional scale but not at a local scale, due to not incorporating turbulent flow equations or delineating conduit pathways/locations. EPM models also cannot simulate flow direction or flow rates within conduits. DF models can simulate karst flow in aquifers if one assumes that flow only occurs in the conduits (i.e. there is no exchange with the matrix) and if the geometry and location of the conduits is fairly well known. DC models are useful when the geometry/location of conduits are unknown, but are limited in their ability to simulate transport processes.

CCPF models simulate karst aquifers by taking into account laminar flow in the matrix, as well as laminar and turbulent flow in conduits, and can simulate flow direction as well as flow rates. CCPF models are also more physically based because conduit physical parameters (e.g. diameters) can be input into the model and exchange flow between the matrix and conduits is accounted for. In this study, the CCPF model MODFLOW-CFP is examined and evaluated at a local and sub-regional scale. Prior to a discussion on the methods and results of the study, a review of previous studies that involve MODFLOW-CFP is necessary.

2.1.2 Previous Studies With MODFLOW-CFP

As mentioned above, MODFLOW-CFP was created by Shoemaker et al. (2007) to simulate flow in karst aquifers with components of conduit and or vuggy porosity. Using cubes of Key Largo Limestone, DiFrenna et al. (2008) experimentally calculated the hydrodynamic threshold between laminar and turbulent flow within the limestone samples. Kuniansky et al. (2008) simulated the experimental results from DiFrenna et al. (2008) using the CFP program. The experimental results were simulated by using mode 2 of the CFP program, which simulates flow in domains with preferential flow layers (often a product of vuggy porosity). Shoemaker et al. (2008) used CFP mode 2 to study the effects of turbulence on hydraulic heads and parameter sensitivities within the Biscayne Aquifer of south Florida. Hill et al. (2010) conducted a local scale study comparing the performance and accuracy of MODFLOW-2005 to CFP by modeling a site near Weeki Wachee, Florida. Discharge and matrix water levels of the karst aquifer were simulated by using CFP mode 1 (which simulates flow in domains where conduits are present). Overall, it was found that the CFP model produced more accurate results than the MODFLOW-

2005 model. However, Hill et al. (2010) attribute this increase in accuracy to the exchange parameter between conduit and matrix, not to the modeling of turbulent flow by CFP.

CHAPTER THREE

OVERVIEW OF THESIS RESEARCH

The primary purpose of this thesis is to evaluate the ability of the new modeling program MODFLOW - Conduit Flow Process (CFP) to accurately simulate groundwater flow in karst aquifers. A secondary purpose of this thesis is to evaluate the ability of the modeling program Modular 3-D Transport Model – Multi Species (MT3DMS) to accurately simulate contaminant transport in karst conditions. This chapter describes the methods, objectives, hypotheses, and significance of this research.

3.1 Methods

3.1.1 Program Code

The primary method used in this study will be the USGS program MODFLOW-CFP. CFP is a modular program that simulates laminar and turbulent flow that occurs in karst aquifers. CFP is meant to work in conjunction with MODFLOW-2005. There are three modes that can be activated within CFP. CFP mode 1 (CFPM1) is in essence a CCPF model, coupling the traditional groundwater flow equation that simulates flow in a porous matrix, with equations that simulate flow in conduit like pipes. CFP mode 2 (CFPM2) simulates turbulent flow in dual porosity aquifers by inserting a high conductivity flow layer that switches between laminar and turbulent flow based on certain hydraulic gradients. CFP mode 3 (CFPM3) simulates turbulent flow by activating CFPM1 & CFPM2 simultaneously (Shoemaker et al., 2007). In this study only CFPM1 will be used, given that the laboratory analog and Woodville Karst Plain only have conduit karst features.

MT3DMS will also be used in this study. MT3DMS is a modular, three dimensional, multi-species, transport model program developed by Zheng & Wang (1999). MT3DMS can simulate contaminant advection, dispersion/diffusion, and chemical reactions in groundwater. MT3DMS is meant to be used in conjunction with a finite difference, block centered flow model such as MODFLOW-2005.

3.1.2 Basic Structure of the Study

To evaluate MODFLOW-CFP, this study was divided into two parts: a laboratory scale study and a sub-regional scale study. In the laboratory scale study, the objective of the study was to determine whether CFP or MODFLOW-2005 could simulate karst flow more accurately. Two groundwater flow models of a laboratory scale karst analog model were created using MODFLOW-2005 and MODFLOW-CFP. Simulated results from both models were then compared to observed conditions in the karst analog model. Since all parameters were known in the analog model, a comparison of residuals was done to determine which model was more accurate. A transport model using MT3DMS was also created based on the karst analog. Simulated transport results were visually compared to observed conditions in the karst analog model. Further details on the laboratory scale study will be presented in the next chapter.

In the sub-regional scale study, the objective of the study was to test the impact turbulent flow can have on simulated heads and discharges and evaluate the importance of including conduits/pipes and their respective parameters (e.g. wall roughness, wall permeability, etc.) in a groundwater model. A groundwater flow model of the Woodville Karst Plain, south of Tallahassee, Florida, was created using CFP. Simulated results of a storm event from the CFP model were then compared to a previous MODFLOW-2000 model by Davis et al. (2010) that simulated the same storm event. A sensitivity study was then performed on various parameters of the model. Further details on the sub-regional scale study will be presented in the next chapter.

3.1.3 Hypotheses

This thesis tests the following hypotheses:

1. MODFLOW-CFP can model flow conditions at a laboratory scale more accurately than MODFLOW-2005.
2. MT3DMS can model contaminant transport at a laboratory scale.
3. For a specific study area, at a sub-regional scale, a MODFLOW-CFP model will produce more accurate transient simulation results than results from an equivalent MODFLOW-2000 model.

3.1.4 Significance

Many groundwater models are EPM models and do not take into account pipe/conduit parameters (e.g. diameter, tortuosity, etc.) or turbulent flow when simulating groundwater flow in karst aquifers. This can lead to errors in simulation results. CFP is a relatively new program that potentially reduces such error by taking into account flow through karst conduits and turbulent flow. The evaluation of CFP in this study is significant because it tests the ability of CFP to simulate flow in karst aquifers and determines at what investigation scale (if any) CFP should be used at.

CHAPTER FOUR

KARST GROUNDWATER MODELS

To evaluate MODFLOW-CFP two studies were performed: a laboratory scale study and a sub-regional scale study. The primary purpose of the laboratory scale study is to determine whether MODFLOW-CFP or MODFLOW-2005 simulates karst conditions more accurately. The primary purpose of the sub-regional scale study objective of the study is to test the impact turbulent flow can have on simulated heads and discharges when compared to an equivalent MODFLOW-2000 model.

4.1 Laboratory Scale Study

4.1.1 Overview

To determine if CFP simulates flow in karst conditions more accurately, two numerical groundwater models based on a laboratory scale karst analog model by Faulkner (2008) were created using CFP and MODFLOW-2005. Faulkner (2008) constructed a laboratory karst analog model that simulated flow in a conduit and matrix domain (Figure 9). The analog model was rectangular and constructed out of Plexiglas, with a 2 cm diameter conduit located at the bottom of the model, and a matrix domain composed of glass sand sized beads overlying the conduit. Overall, the analog model was 60 cm long, 26 cm wide, and 2 cm thick. The interior of the matrix domain, including the inflow and outflow reservoirs was 57.8 cm long, 24.1 cm wide, and 2 cm thick. The conduit portion of the analog model was 57.8 cm long, 2 cm wide, and 2 cm thick. A stainless steel screen separated the conduit from the matrix, but allowed the exchange of water flow and solutes between the two domains. Two matrix water reservoirs bounded two sides of the matrix domain. Pressure transducers were placed in both domains to measure hydraulic head. Multiple experiments were conducted to measure hydraulic head distribution and contaminant transport. Two general cases were examined by Faulkner: Conduit head greater than Matrix head (case 1), and Matrix head greater than Conduit head (case 2). Hua (2009) used a Navier-Stokes based code to create a CCPF numerical model of Faulkner's karst analog, and was able to successfully simulate the head distribution and contaminant transport for the case 1 experimental results.

In this laboratory scale study, only case 1 (conduit head greater than matrix head) was simulated using CFP and MODFLOW-2005. Case 2 was not simulated as there were problems with the observed results in the analog model. For case 1, residuals of the CFP, MODFLOW-2005, and Navier-Stokes model by Hua (2009) were compared to determine which model most accurately simulated the flow within the karst analog. MT3DMS was then used to simulate the contaminant transport within the karst analog. Results from MT3DMS were compared to transport simulation results from Hua (2009).

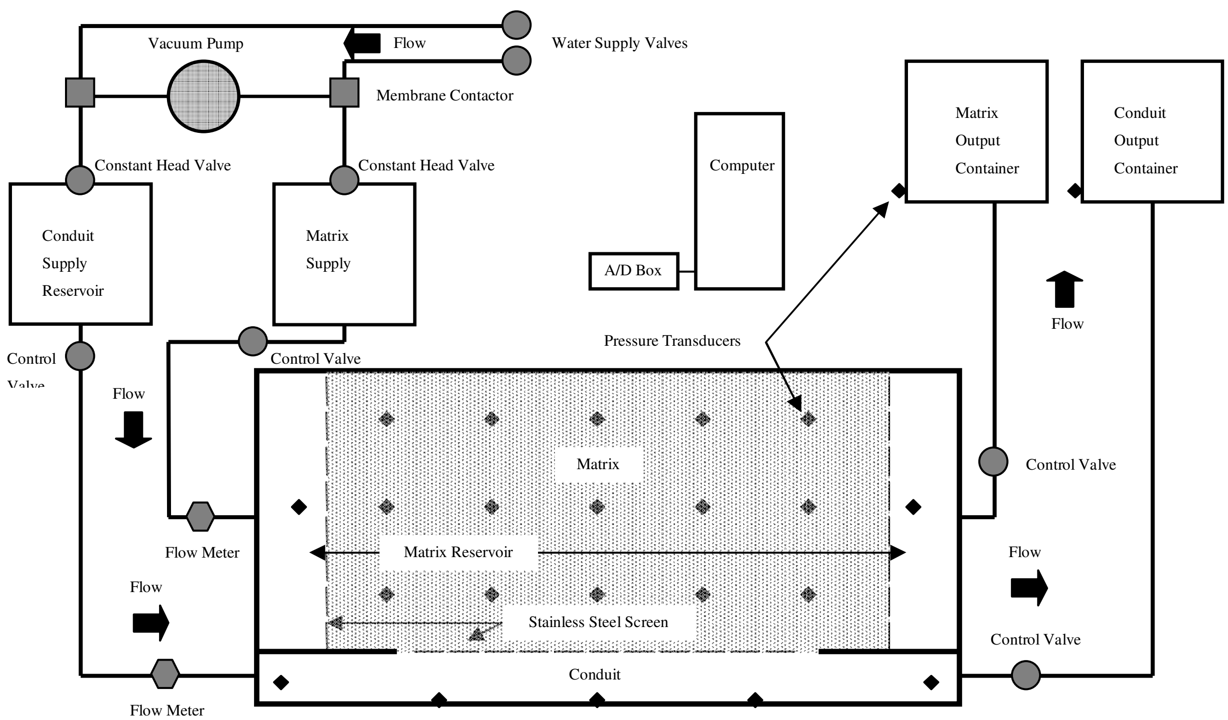

Figure 9: Diagram of the laboratory scale karst analog model. Figure is modified from Faulkner et al. (2009).

4.1.2 Conceptual Models

For this study, one conceptual model was used for both the CFP and MODFLOW-2005 numerical models (Figure 10). Model boundaries were chosen to coincide with the 4 sides of the analog model. Flow was occurred from left to right. The matrix water reservoirs, located on the left and right side of the analog model, were set as constant head boundaries for the matrix domain. The inlet and outlet portions of the conduit were also defined as constant head boundaries for the conduit domain. The top and bottom of the analog model were set as no-flow boundaries. Overall as a system, the analog model was considered to be a confined aquifer under steady state conditions, with no recharge.

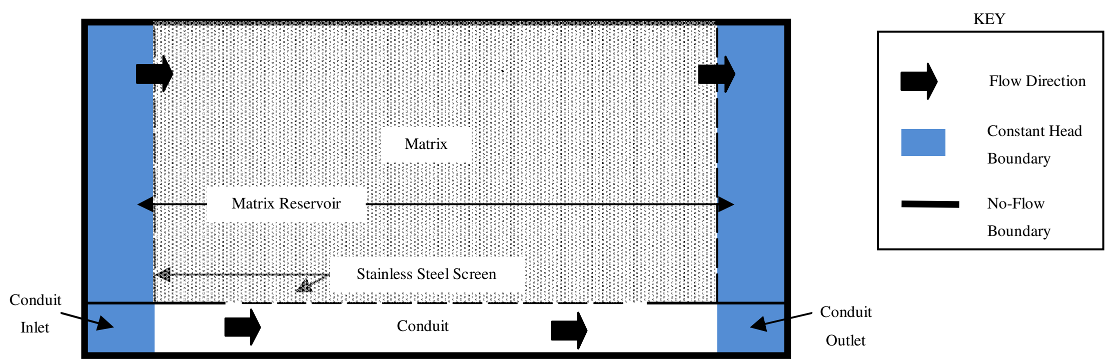

Figure 10: Conceptual model of the laboratory scale model. This was used to create the MODFLOW-2005 and MODFLOW-CFP models. Diagram is not to scale. Modified from Faulkner et al. (2009).

4.1.3 Numerical Models

Of the three modes available in MODFLOW-CFP, CFPM1 was used to create the CFP numerical model of the karst analog (Figure 11). The model has 1 row, 10 columns, and 6 layers. Matrix hydraulic conductivity is set at 0.0619 cm/s. The left constant head boundary for the matrix domain is set at 29.94 cm and the right constant head boundary for the matrix domain is set at 23.66 cm. For the conduit, a pipe network of 10 pipe nodes and 9 pipes was created. Water temperature within the pipe network is set to 19.8 degrees Celsius. All pipe nodes are assigned to the centers of their respective model cells. The left (inlet) constant head pipe node is set to 32.51 cm, and the right (outlet) constant head pipe node is set to 32.49 cm. All other pipe nodes are set as variable head nodes. All pipe segments have a diameter of 2 cm, tortuosity of 1.0, roughness of 0.00001, lower critical Reynolds number of 4000, and upper critical Reynolds number of

12,000. Surface dependent exchange in the pipe network is active, with pipe wall permeability set at 0.0619 cm/s.

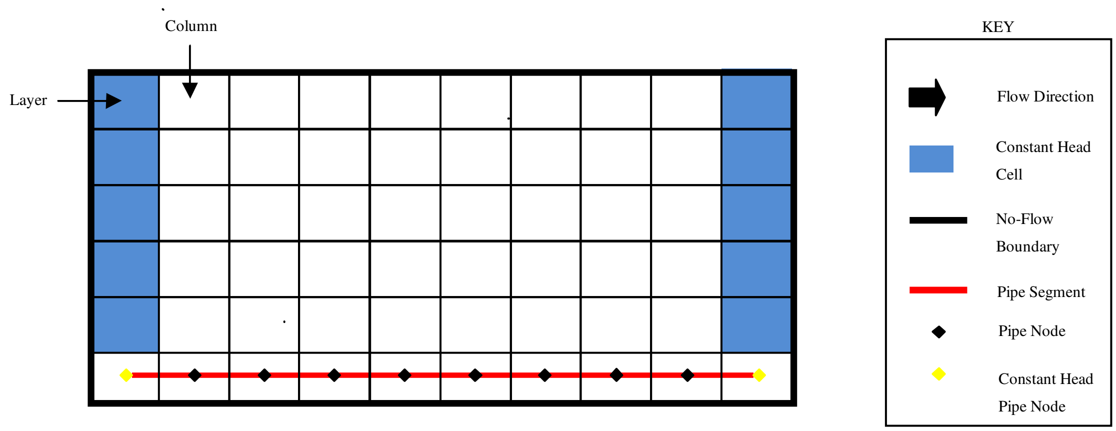

Figure 11: CFP numerical model of the laboratory scale model. Diagram not to scale.

The MODFLOW-2005 numerical model is almost identical to the CFP numerical model with several minor differences (Figure 12). Instead of a pipe network, an extra layer was used to represent the conduit. Therefore the MODFLOW-2005 model has 1 row, 10 columns and 7 layers, with the 7th layer having a high hydraulic conductivity (K) to simulate flow within the conduit. The hydraulic conductivity of the 7th layer was calculated by hand to be 12179.56 cm/s. This calculation was based on combining the Darcy's Law Equation with the Poiseuilles Law Equation, and solving for hydraulic conductivity. Constant head cells were also used for the inlet and outlet portions of the 7th layer, instead of constant head pipe nodes

4.1.4 Model Calibration

Given the simple nature of the karst analog model and the fact that all parameters were known for the karst analog model, calibration of the CFP and MODFLOW-2005 numerical models was not required. A copy of the CFP input file is attached in Appendix A.

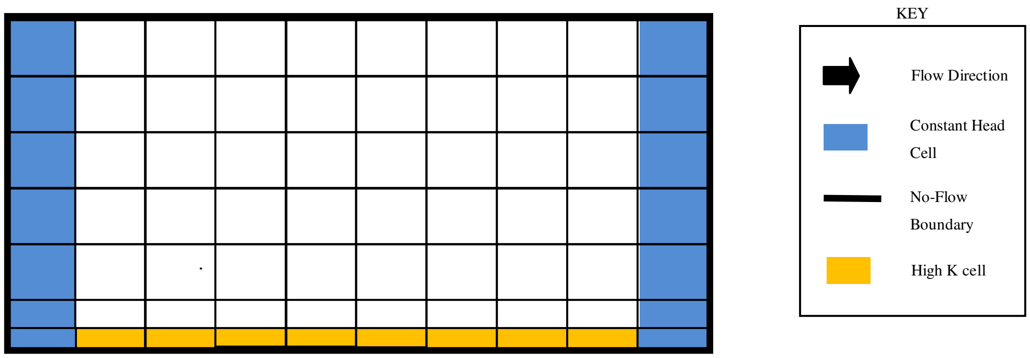

Figure 12: MODFLOW-2005 numerical model of the laboratory scale model. Diagram is not to scale.

4.1.5 Simulation Results

Head measurements from the analog karst aquifer model are shown below in Figure 13a. Contours of the head distribution in the analog model were generated by ArcGIS, but will not be considered in this study. Figure 13b shows head distribution contours based on the output simulation data from the CFP model. Contours in Figure 13b were generated using the program Surfer. The contour interval in Figure 13b is 0.5 cm. Based purely on a visual inspection of the observed vs. simulated results, it is apparent from Figure 13 that the CFP model reasonably simulates groundwater flow in the analog karst model. The simulation results show higher head values in the conduit, relative to the matrix, and that water flows from the conduit up into the matrix. The simulation also shows that flow in the matrix occurs from left to right. These simulation results correspond with the observed head values in the analog model. While a visual inspection of the results indicates that the CFP model reasonably simulates flow in the analog model, a more in depth analysis of the results is required to determine how well the numerical model simulates the analog model. This analysis is discussed in the next section.

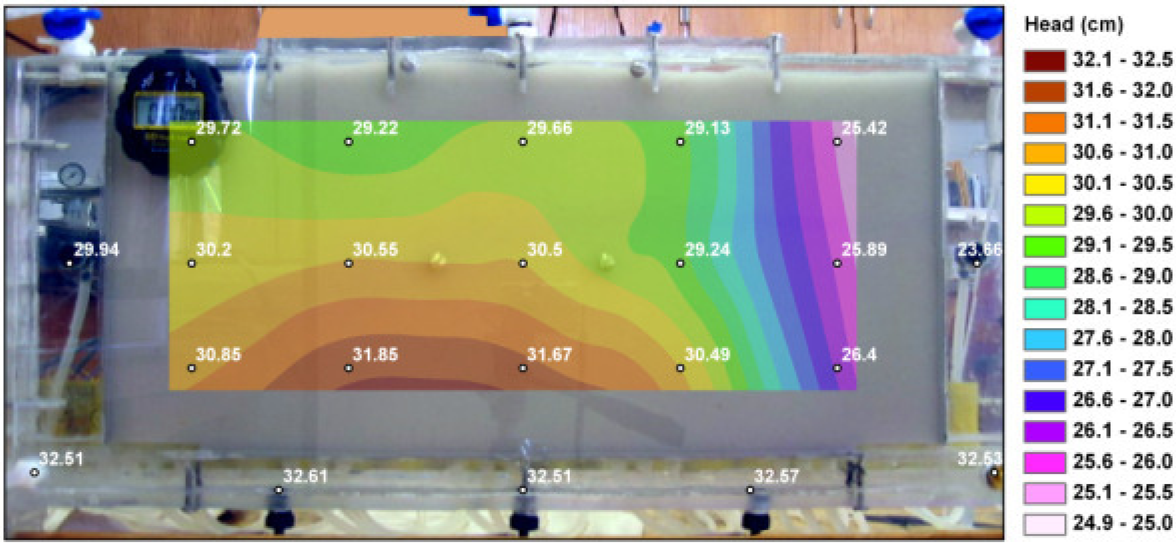

13a.

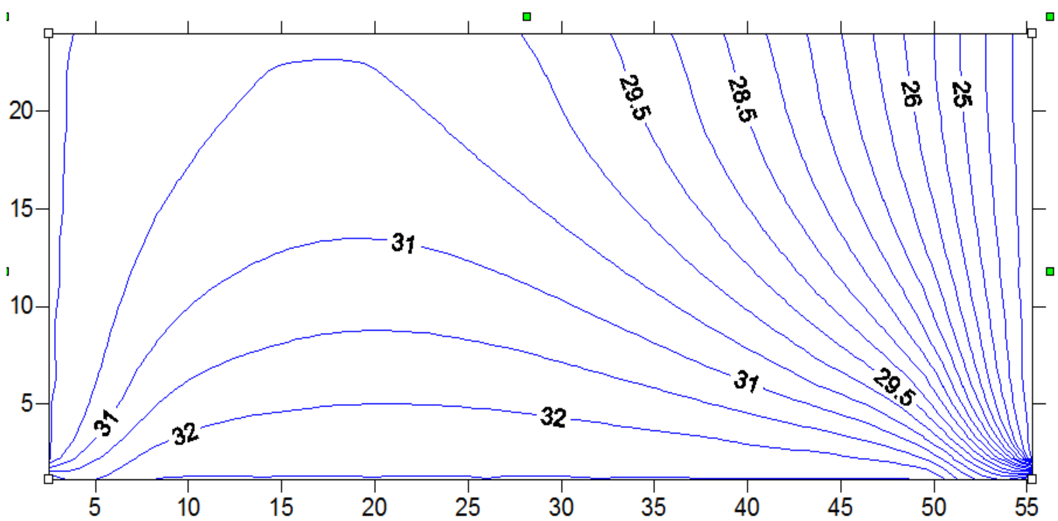

13b.

Figure 13: Laboratory Scale Simulation Results. a.) Head distribution results from karst analog model - numbers in white are measured head values. Colored contour lines represent head contours. Modified from Faulkner et al. (2009); b.) Contour lines of CFP simulated head with a contour interval of 0.5 cm – axes are in cm and represent the spatial dimensions of the model.

Standard deviation for each transducer in the analog model was calculated by Faulkner (2008). These standard deviation values were used in this study to calculate variance values for each analog transducer. Variance was then used to calculate weights for the analog observation values, as well as the corresponding simulation and residual values (Note: residual = observed – simulated). Once weights were assigned to the simulated, observed, and residual values, graphs were plotted, showing the weighted data. Figure 14a is a graph of the weighted simulated vs weighted observed data. Figure 14b is a graph of the weighted simulated vs weighted residual data. The linear trend of the data in Figure 14a (with slope of 1) indicates that the simulated values are close to the observed values in the analog model. Figure 14a provides confirmation that the CFP model adequately simulates the analog model. However, weighted simulated vs. weighted observed graphs can often hide data trends/biases. Weighted simulated vs weighted residual graphs can reveal such trends/biases.

In Figure 14b, certain such biases in the data are noted. For example, data points are unequally distributed about the zero weighted residual line, and tend to clump below the zero axis. This indicates that the weighted residual mean is not zero. The calculated weighted residual mean is in fact -0.11. This negative mean value indicates that the simulated results are larger than the observed values, showing us that the CFP model is generating simulation results that overestimate the observed head values.

The two examples of trends/biases discussed above indicate that there is some error in the model. One probable source of that error is the boundaries used in the numerical model. Constant head boundaries were used for the matrix portion of the domain because of the presence of the matrix inflow and outflow reservoirs. The reservoirs were not filled with glass beads, and there was only one transducer per reservoir. There was uncertainty in the beginning of this study on how best to model the reservoirs. To make the modeling simple, the reservoirs were assumed to have constant head and were defined as boundaries. The problem with this assumption however, is that head variation within the reservoirs is ignored. The error was introduced into the model and was not considered. A possible remedy for this error could be to change the reservoirs into specific flux (Neumann) boundaries, using the inflow and outflow flux measurements from the analog model.

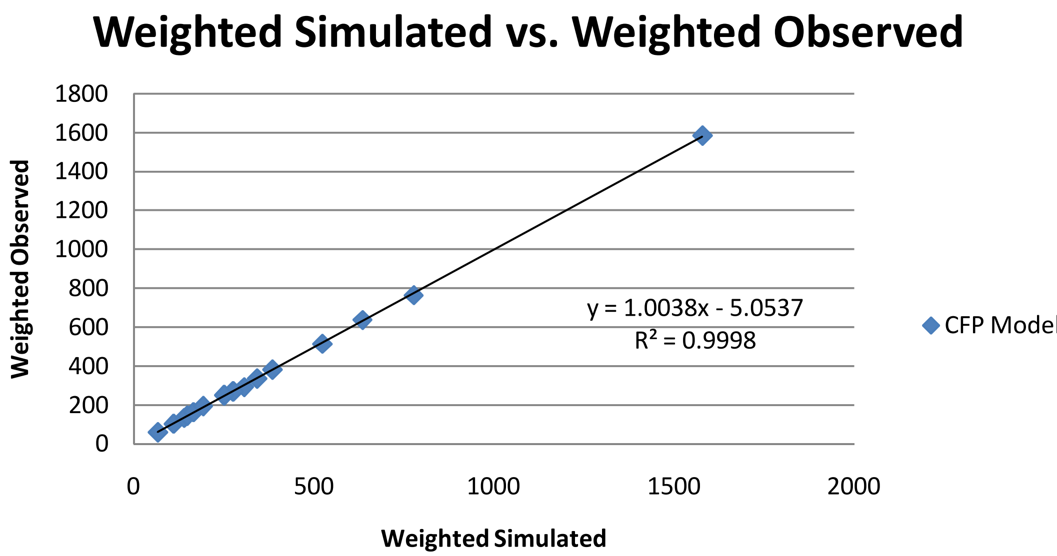

14a.

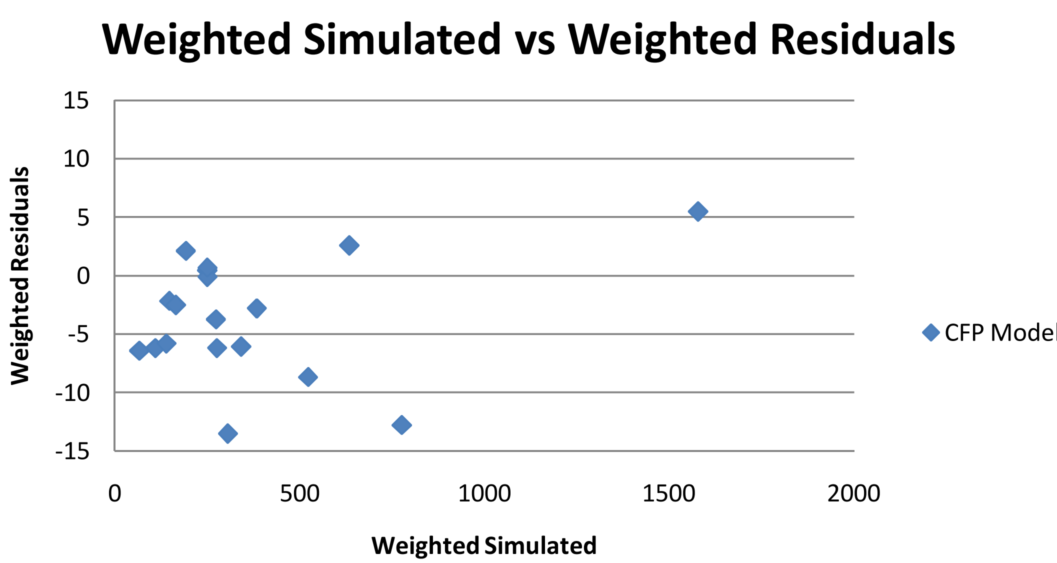

14b.

Figure 14: Graphs of Simulated Hydraulic Head. a.) Weighted Simulated Heads vs. Weighted Observed Graph; b.) Weighted Simulated Head vs. Weighted Residuals.

Mean values for residuals and weighted residuals, as well as variance were calculated. Results are shown in Table 1 & 2 below. Of the three models, CFP has the lowest residuals, indicating that CFP simulated the karst analog more accurately than MODFLOW-2005 and even Hua's Model.

Table 1: Residual Table for Laboratory Scale Study. Table showes residual means and residual variance of the CFP, MODFLOW-2005 (MF2K5), and Navier Stokes Model (Hua Model).

Model Type	Residual Mean	Residual Absolute Mean	Residual Variance
CFP	-0.55	0.63	0.59
MF2K5	-0.61	0.66	0.65
Hua Model	-0.71	0.77	0.57

Table 2: Weighted Residual Table for Laboratory Scale Study. Table showes weighted residual means and weighted residual variance of the CFP, MODFLOW-2005 (MF2K5), and Navier Stokes Model (Hua Model).

Model Type	Weighted Residual Mean	Weighted Residual Absolute Mean	Weighted Residual Variance
CFP	-3.63	4.90	26.20
MF2K5	-4.39	4.79	22.55
Hua Model	-7.38	7.80	71.28

MT3DMS was used to simulate contaminant transport within the karst analog, based on a dye experiment by Faulkner (2008). Simulation results were visually compared to Faulkner's observed results in the karst analog. Simulation results are shown in Figure 15 below. While not exceptional, the results indicate that MT3DMS can fairly simulate transport within a karst at a laboratory scale.

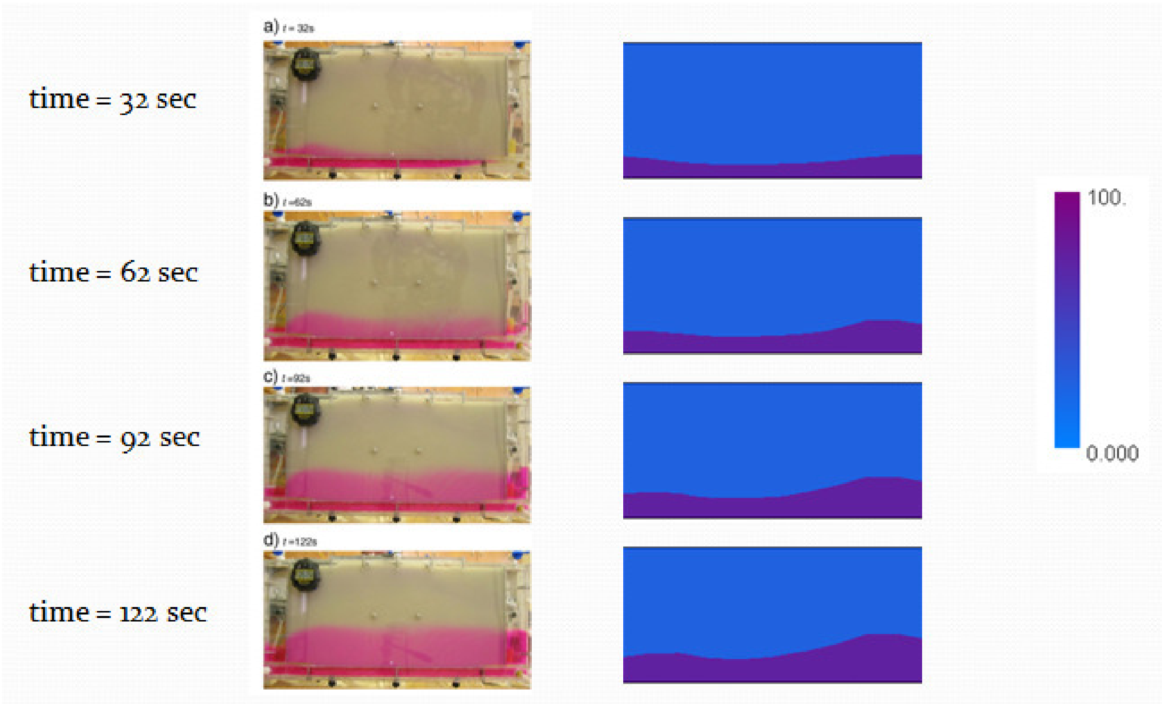

Figure 15: MT3DMS simulation results. Left column shows dye experiment from Faulkner (2008) over a period of 4 time intervals, with each interval being 30 seconds long. The right column shows the MT3DMS simulation of the plume for the same time periods.

While a contaminant transport code is not yet available for CFPM1, a transport code was recently developed by Shoemaker for CFPM2. This code was also applied to the dye experiment by Faulkner (2008). However, attempts to model the dye plume failed (Figure 16). Dye transport did not travel as fast as that observed in the analog. This failure to simulate the dye transport may be a result of problems with the code. However a more likely cause is that of improper use of CFPM2, which is meant to be applied to karsts with vuggy porosity, not conduit porosity.

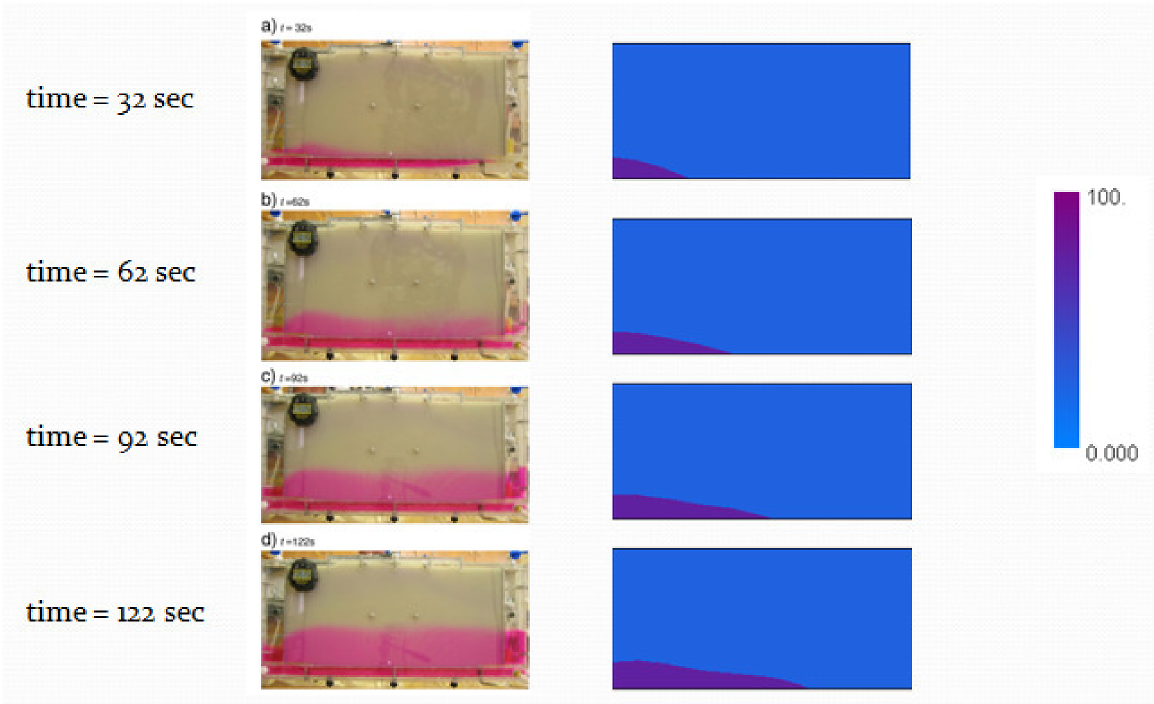

Figure 16: CFP mode 2 simulation results. Left column shows dye experiment from Faulkner (2008) over a period of 4 time intervals, with each interval being 30 seconds long. The right column shows the CFPM2 based transport code simulation of the plume for the same time periods.

4.2 Sub-Regional Scale Study

4.2.1 Overview

To test the impact turbulent flow can have on simulated heads and discharges, a sub-regional model of the Woodville Karst Plain was created using CFP. This model is based on a previous MODFLOW-2000 model by Davis et al. (2010). The EPM model by Davis et al. (2010) was created to simulate groundwater flow and nitrate fate and transport within the Woodville Karst Plain, south of Tallahassee. To account for flow in submerged karst caves within the Woodville Karst Plain, Davis et al. (2010) used high hydraulic conductivity cells to create a "cave network" where cave flow was simulated. As discussed in chapter 1 and 2 of this thesis, EPM models can simulate karst flow. However such models are prone to error since EPM models do not use pipe flow equations to account for flow through pipe like caves, or account for turbulent flow. The question then arises: can EPM models adequately simulate flow in karst aquifers at a sub-regional scale? The purpose of this study is to answer that question by determining if there is a substantial difference in simulation results between an EPM model that does not account for turbulent flow and a CFP model that does account for turbulent flow.

4.2.2 Sub-regional Geology and Hydrogeology

In this study the extent of the sub-regional model encompasses the Woodville Karst Plain, a geographic area south of Tallahassee, Florida, characterized by prominent karst features such as sinking streams, sink holes, submerged caves systems, and springs. Figure 17 shows the geographic extent of the Woodville Karst Plain.

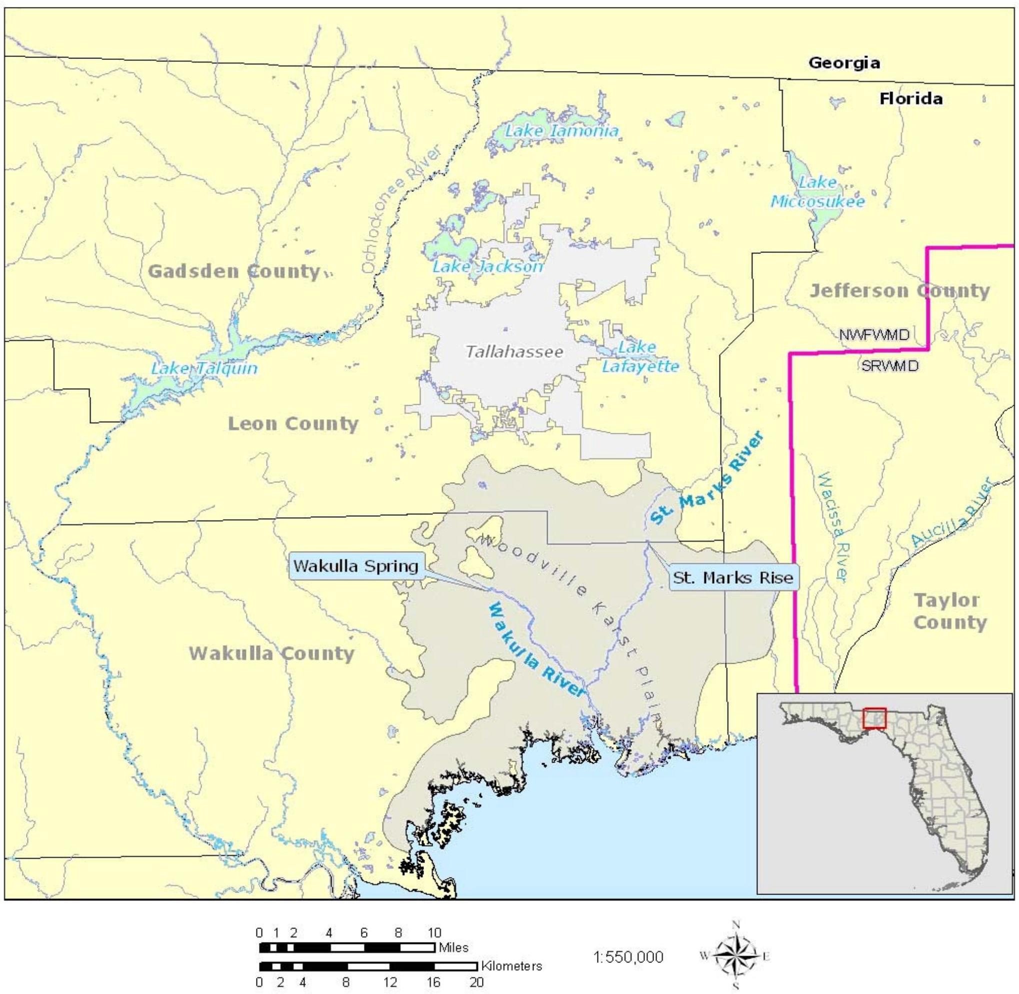

Figure 17: Geographic Extent of the Woodville Karst Plain. From Barrios (2006).

The Woodville Karst Plain is underlain by Paleogene to Quaternary sedimentary rocks. At the base, the Paleocene Clayton Formation, a calcareous marine clay, acts as a no flow boundary. Above the Clayton Formation are the Eocene Oldsmar, Avon Park, and Ocala Formations, which are all comprised of permeable limestone, at least in the surrounding Tallahassee area. Above these three formations are the relatively thin Miocene St. Marks /Chattahoochee Formations. The St. Marks is limestone that has been partially dolomitized. The Chattahoochee is primarily a dolostone, with limestone, chert, sand, clay, heavy minerals, & phosphates. The hydraulic properties of these two formations ranges from permeable to impermeable. Above the St. Marks/Chattahoochee Formations is the Hawthorn Group, a primarily sand and clay unit that can serve as a confining layer in certain areas. There are other sedimentary formations younger than the Hawthorn Group, however they will not be discussed in this study. For further information see Davis & Katz (2007). A Stratigraphic column of the study area is presented below in Figure 18.

SYS-TEM	SERIES	GEOLOGIC UNIT	HYDROGEOLOGIC UNIT	MODEL LAYERS	
				Davis et al. (2010)	Sub-regional model (This study)
QUATERNARY	HOLO-CENE	Undifferentiated deposits	Water-table aquifer	Not simulated (Generally not present)	Not simulated (Generally not present)
	PLEIS-TOCENE	Undifferentiated terrace and shallow marine deposits			
TERTIARY	PLIO-CENE	Miccosukee Formation			
	MIOCENE	Hawthorn Group	Hawthorn Clays	Not simulated (Generally not present)	Not simulated (Generally not present)
		Chattahoochee and St. Marks Formations	Upper Floridan aquifer	Layers 1 and 2	Layers 1 and 2
	OLIGOCENE	Suwannee Limestone			
	EOCENE	Ocala Limestone			
		Avon Park Formation			
		Oldsmar Formation			
	PALEOCENE	Clayton Formation	Low-permeability sediments	No-flow boundary	No-flow boundary

Figure 18: Stratigraphic Column of the Woodville Karst Plain. Figure modified from Davis et al. (2010).

In the region of Tallahassee there are two aquifers: the Water Table Aquifer and the Upper Floridan Aquifer. The Water Table aquifer is found a few feet below the surface and does not yield much water. It will not be considered in this study. The Oldsmar to Chattahoochee/St. Marks formations are the lithologic units that make up the Upper Floridan Aquifer, with the Clayton Formation and Hawthorn Group acting as the bottom and top confining layers (Figure 18). The Upper Floridan Aquifer is the primary source of drinking water in the Tallahassee Area. A cross section of the aquifer can be seen below (Figure 19).

Flow in general is from north to south, largely due to the high potentiometric surface in the north and northwest of Tallahassee (Figure 20). This potentiometric high surface is due to the low effective porosity limestone sediments deposited in the Suwannee Straits. The thick layer of overlying Hawthorn Group sediments above the Straits has also prevented water from infiltrating into the deep subsurface, thus keeping effective porosity low. Where the Hawthorn layer is thick (primarily over the Suwannee Straits) surface water runoff is high, forming numerous streams. Where the Hawthorn Group is thin or even absent (such as the Woodville Karst Plain), water is able to easily and quickly infiltrate, dissolving the underlying limestone, forming substantial networks of conduits and sinkholes. A lack of streams is easily noticed in such areas.

As a result of infiltration and dissolution of limestone in the Woodville Karst Plain, an extensive network of submerged cave/conduit networks exists, through which a substantial amount of water flows. Though multiple springs exist within the Woodville Karst Plain, the three primary discharge points for the cave networks are Wakulla Spring, Spring Creek Springs Group, and St Marks Spring. With respect to Wakulla Spring, approximately 37 miles of cave networks that connect to the spring have been explored and mapped by cave divers (Davis et al., 2010, p. 8). Figure 21 shows the extent of mapped cave networks. Groundwater flow within these caves is complex and not fully understood. In general water enters the caves from the surface and is discharged at Wakulla Spring. A groundwater divide exists at the intersection of the R tunnel with the O and K tunnels (Kincaid, 1999). Some water from the R tunnel flows north and discharges at Wakulla, while the rest of the water flows south and eventually discharges at Spring Creek Group Spring(s). At times the groundwater divide can shift or disappear such that flow from Spring Creek Springs Group is diverted to Wakulla Spring.

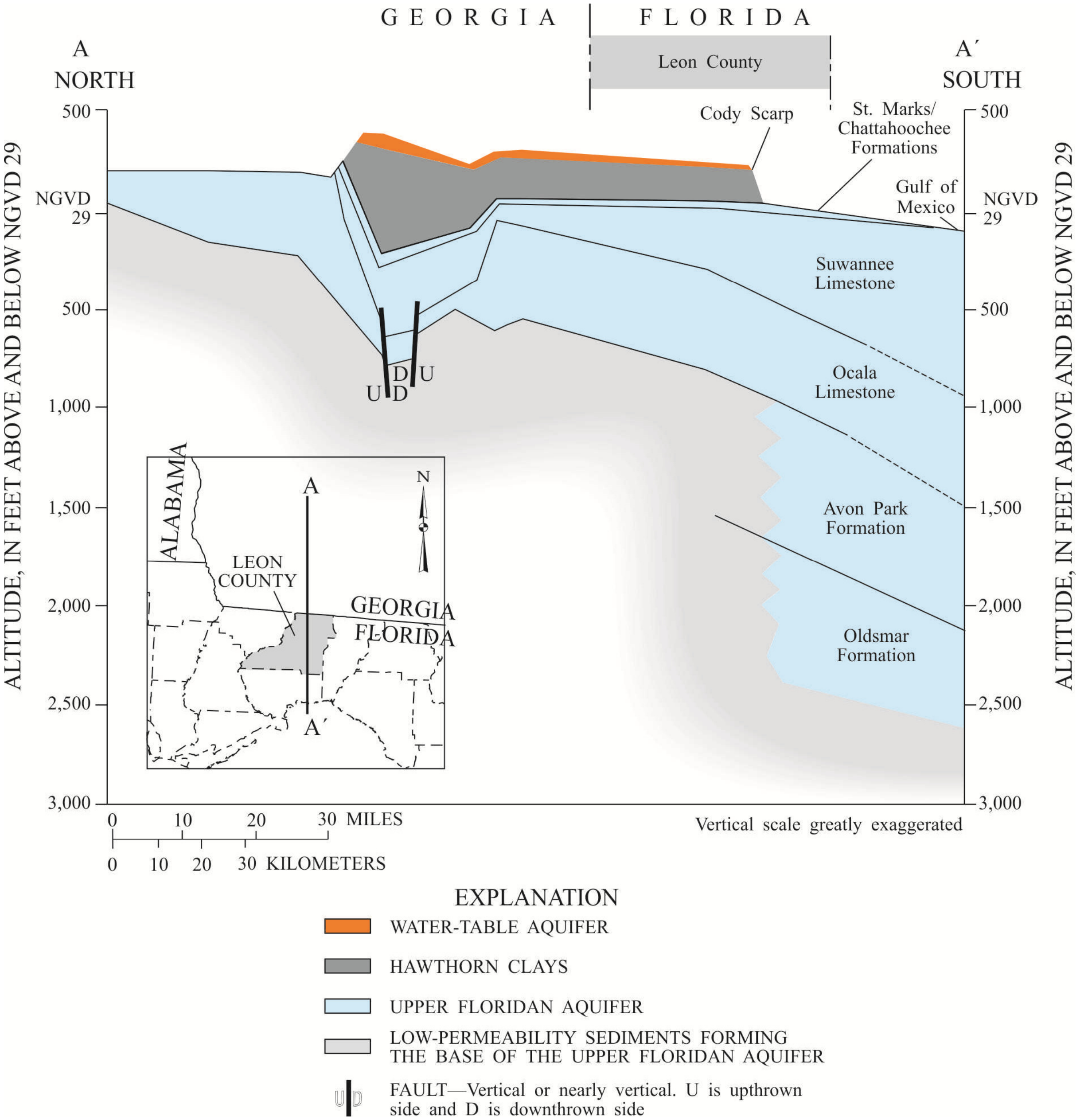

Figure 19: Geologic cross section of Leon County, Florida. The southern half of the cross section is the Woodville Karst Plain. Figure from Davis & Katz (2007).

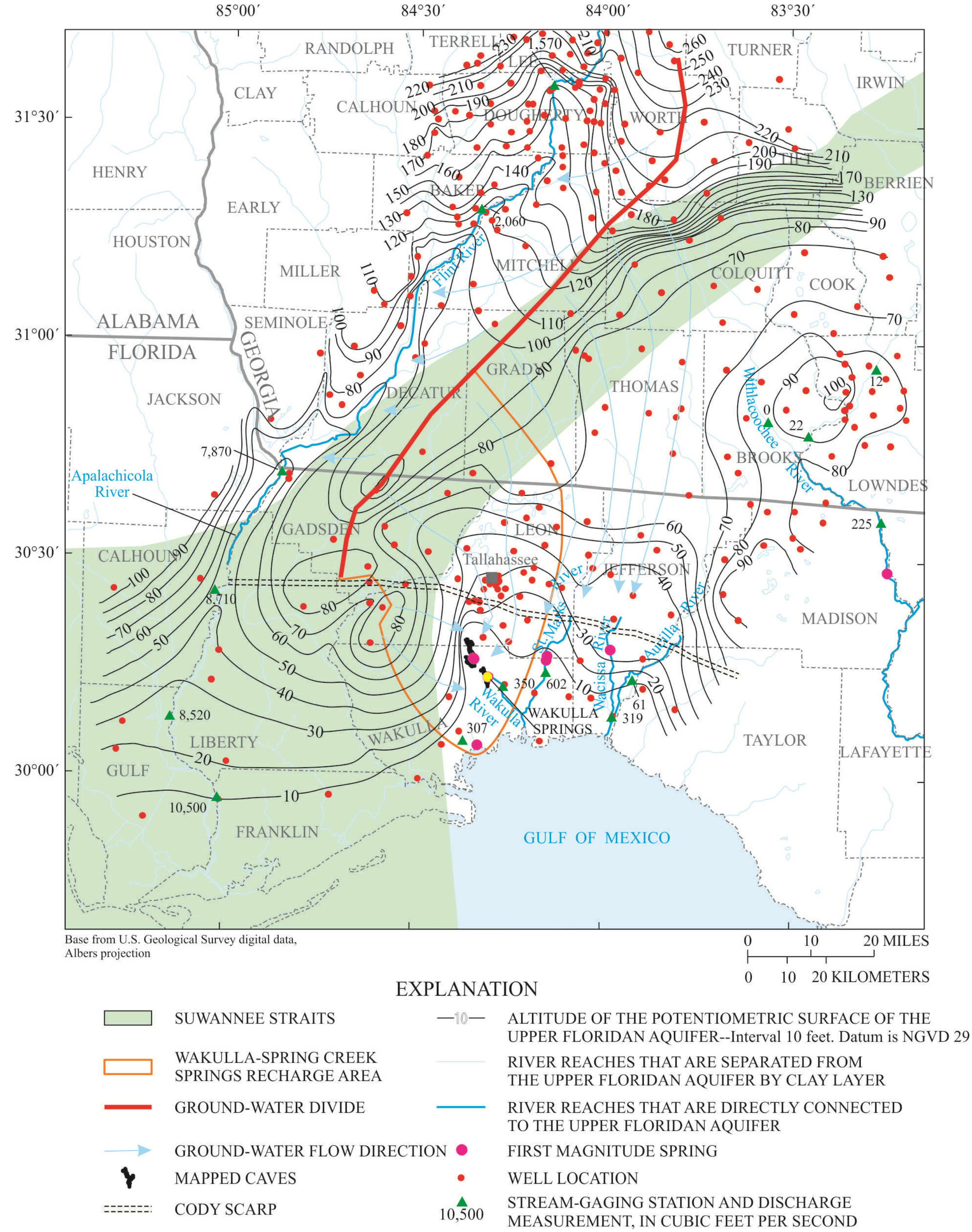

Figure 20: Potentiometric surface map of Northwest Florida. From Davis & Katz (2007).

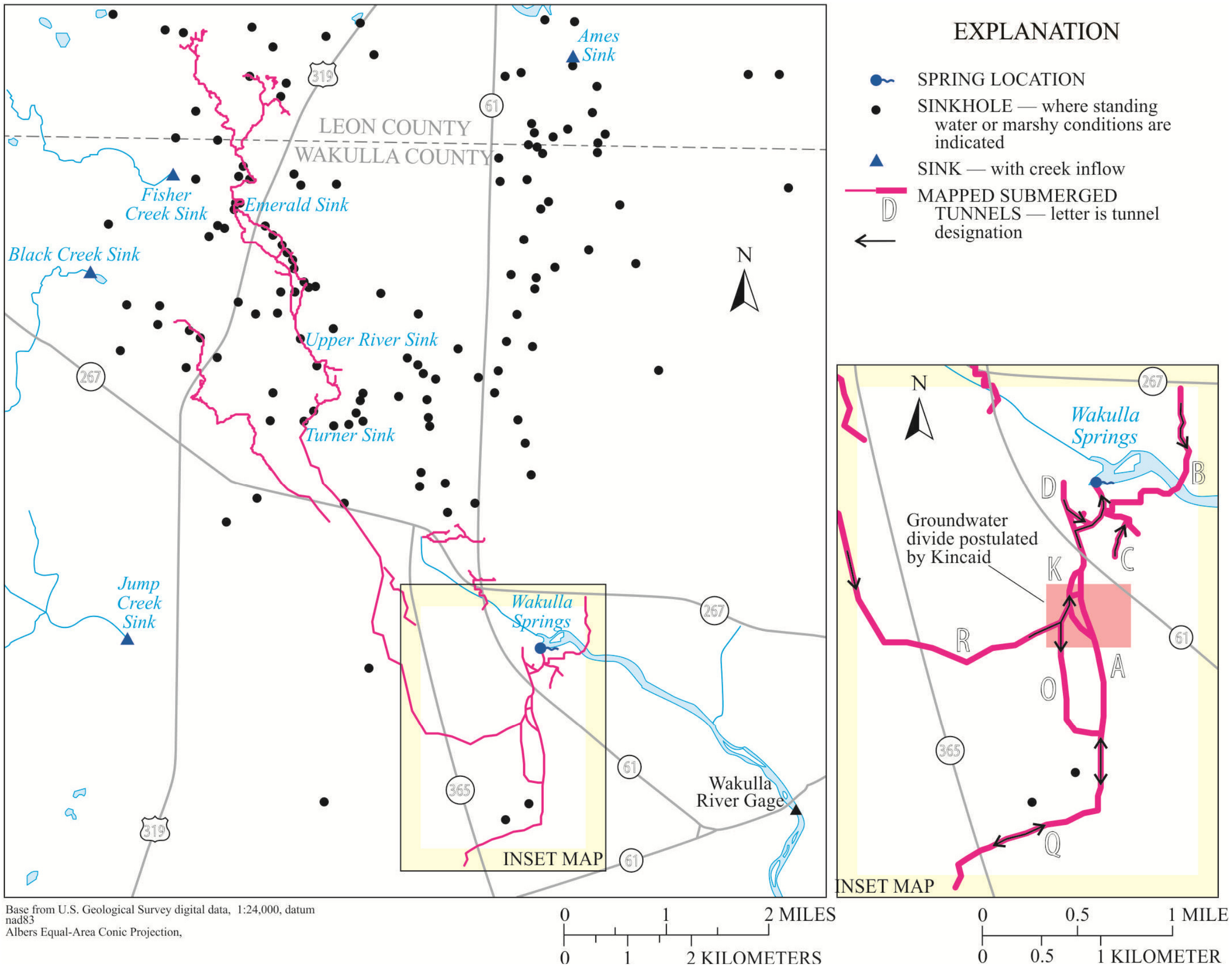

Figure 21: Map of explored and mapped caves systems in the Woodville Karst Plain. Note that the mapped caves make up only a small part of the entire Woodville Karst Plain. The geographic location and extent of most karst features such as caves or conduits are unknown. Figure from Davis et al. (2010).

4.2.3 Conceptual Model

In this study the conceptual model is mainly based on the conceptual model used by Davis et al. (2010). Figure 22 shows the extent of the model outlined in black and also shows regional groundwater flow from the north in Georgia, to the south into the Gulf of Mexico. Figure 23 shows the conceptual model for this study. The conceptual model is divided into four geological/hydrogeological layers: the Hawthorn Group, a sand layer, the Upper Floridan Aquifer (consisting of the Suwannee Limestone, Ocala Limestone, Avon Park Formation, and Oldsmar Formation), and the low permeability sediments layer. The north boundary is a

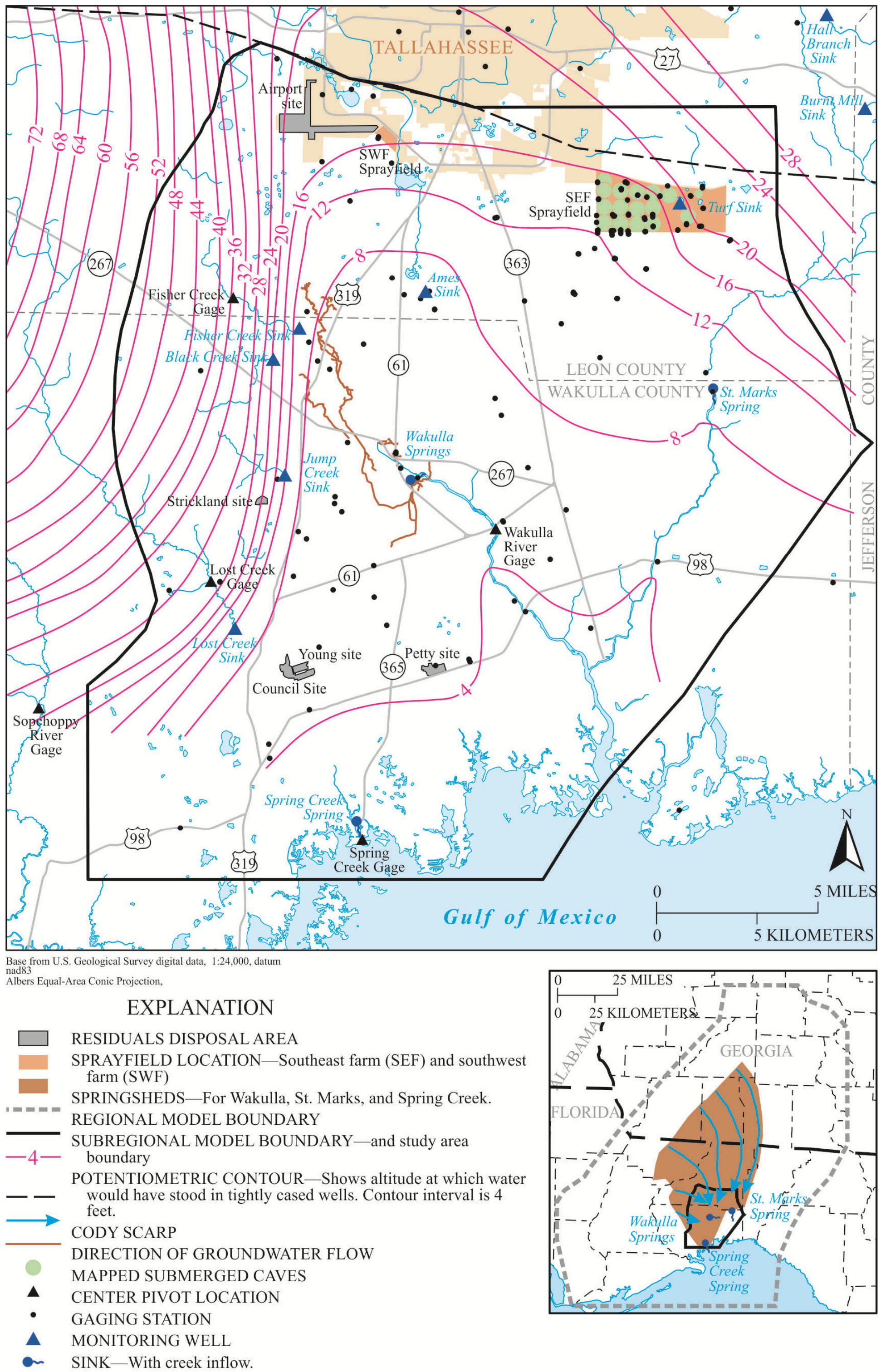

Figure 22: Extent of the sub-regional model. Model boundary is outlined by the bold black line. The lower right map inset shows regional groundwater flow. Figure from Davis et al. 2010.

specified head boundary, while the lower boundary between the Upper Floridan Aquifer and low permeability sediments is a no flow boundary. The south boundary along the Gulf of Mexico is also a no flow boundary. Dissolution of limestone is assumed to occur throughout the model, forming sinkholes, conduits, and caves, with water flowing through these karst features. Sand and clay is assumed to infill the upper portion of the aquifer (layer 1) resulting in a lower hydraulic conductivity. The lower portion of the aquifer (layer 2) has little to no infilling, resulting in higher hydraulic conductivities. The model domain is considered to be a confined aquifer. Sources of recharge include: lateral inflow across the model boundaries, net precipitation, creek flow into sinkholes, irrigation, and discharges into the aquifer from onsite sewage disposal systems (e.g. septic tanks systems). Discharge is assumed to occur only at conduit/cave fed springs and at the boundary that represents the Gulf of Mexico. Regarding the springs, only three discharge points are accounted for in the model: Wakulla Spring, Spring Creek Springs Group, and St Marks Spring. Instead of high hydraulic conductivity cells, a pipe network was used to represent the submerged caves that recharge the three springs.

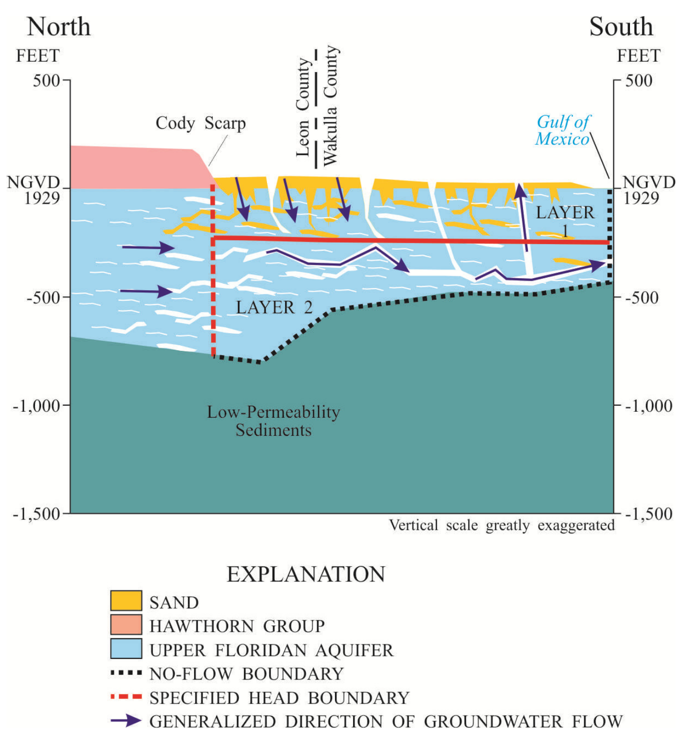

Figure 23: Conceptual model for the Sub-Regional CFP model. From Davis et al. (2010).

4.2.4 Numerical Model

In this study MODFLOW-CFP was used to create a sub-regional model of the Woodville Karst Plain. The sub-regional model in this study is based on a MODFLOW-2000 sub-regional model by Davis et al. (2010). The sub-regional MODFLOW-2000 model by Davis et al. (2010) is based on a previous regional model of Florida and Georgia, by Davis and Katz (2007). The CFP model in this study is almost identical to the sub-regional model by Davis et al. (2010). The primary difference is that pipe networks were incorporated into the original sub-regional model, replacing the high hydraulic conductivity network that Davis et al. used to simulate the subsurface caves.

The sub-regional CFP model consists of 288 rows and 258 columns. Model cells are 500ft by 500ft horizontally. Top and bottom elevations for the cells were derived from the regional model by Davis and Katz (2007). Corresponding to the conceptual model, the CFP model only has two layers. Layer 1 represents the upper portion of the Upper Floridan Aquifer, where hydraulic conductivities are low. Layer 2 represents the lower portion of the Upper Floridan Aquifer, where hydraulic conductivities are high. For each model layer there are 4 specified head boundaries and one no-flow boundary (Figure 24). The base of layer 2 is also considered as a no-flow boundary (not shown in Figure 24). Rivers are simulated using the Drain package (Harbaugh et al., 2000). Hydraulic conductivity values are based on the calibrated values from Davis et al. (2010). Hydraulic conductivities for layer 1 range from 6 to 5,000 ft/day. Hydraulic conductivities for layer 2 range from 10 to 30,000 ft/day. Recharge in the model comes from 5 sources: Inflow across lateral boundaries of the model, net precipitation, creek flow into sinkholes, irrigation at sprayfields, and discharges from onsite sewage disposal systems (e.g. septic tanks). The specified heads at the boundaries were used to simulate the lateral inflow across the boundaries. The Recharge Package (Harbaugh et al., 2000) was used to simulate net precipitation and recharge from irrigation. The Well Package was used to simulate creek flow into sinkholes and discharges from onsite sewage disposal systems. Recharge values used in the CFP model were the same as those used in the MODFLOW 2000 model by Davis et al. (2010). See Table 5 of Davis et al. (2010) for exact recharge values.

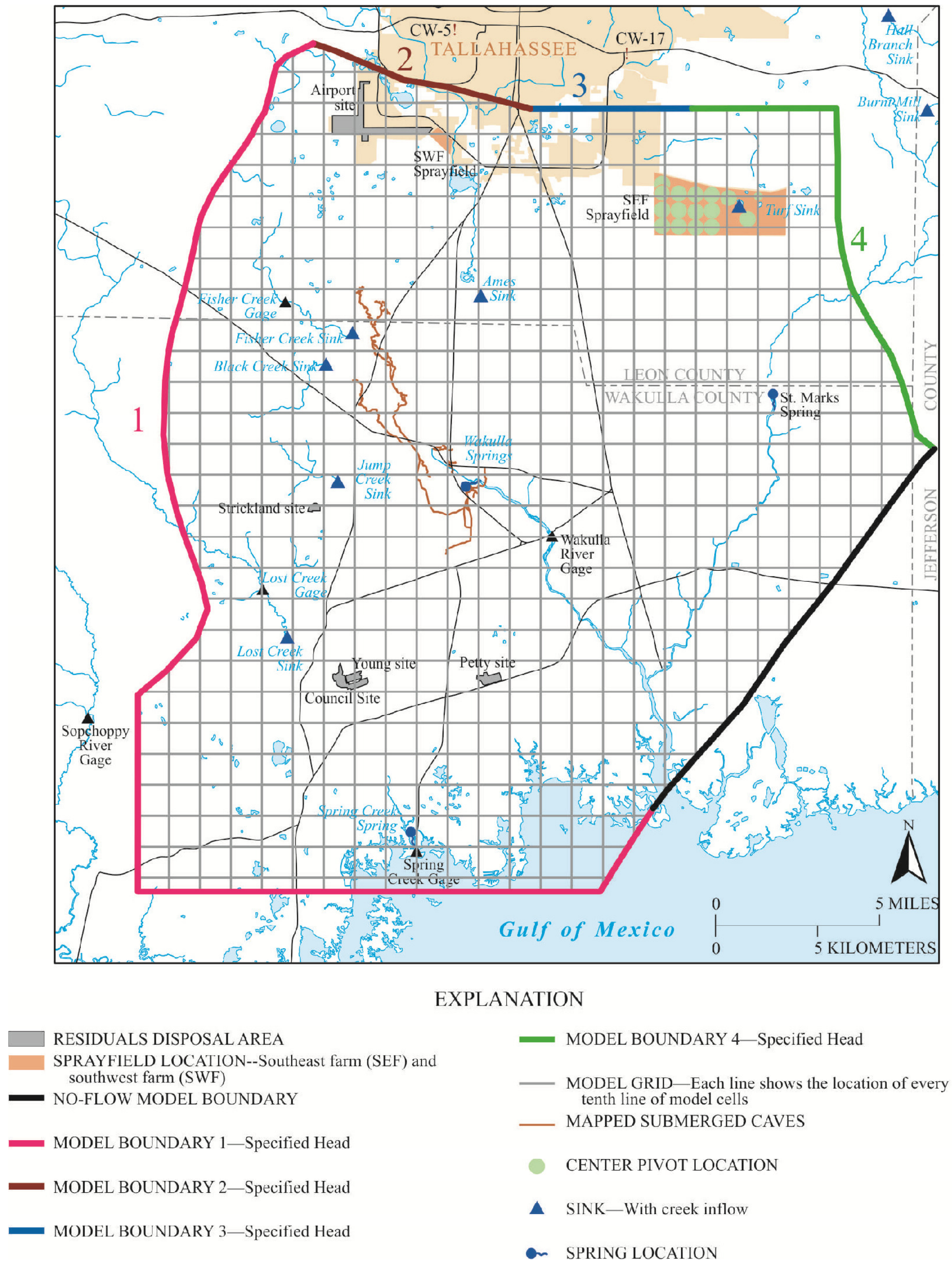

Figure 24: CFP numerical model of the Woodville Karst Plain. Figure shows grid spacing and model boundaries for a single layer. Every tenth cell boundary is shown. Modified from Davis et al. (2010).

In the original sub-regional model, Davis et al. (2010) used a network of very high hydraulic conductivity cells to simulate submerged conduits and caves. In this study a pipe network was created using MODFLOW-CFP (Shoemaker et al. 2007) to replace the very high hydraulic conductivity cells from Davis et al. (2010). Figure 25 shows the original network of very high hydraulic conductivity cells used by Davis et al. (2010). Only a small portion of the very high conductivity cells are based on actual mapped caves. The remaining very high conductivity cells were placed in their respective locations based on inference from field observations that indicated probable cave locations. These observations included: the presence of numerous sinkholes indicating heavy dissolution in the subsurface; a tracer test from Turf Sink to Wakulla Springs with a travel time of about 40 days which indicated a cave or pathway between the two locations; high tannic flows at Lost Creek Sink resulting in tannic flows at Spring Creek Springs Group which indicated a hydraulic connection; and cave diver observations at the southernmost tip of the explored Wakulla caves system that water was flowing southward, indicating a connection between Wakulla Springs and the Spring Creek Springs Group (Davis et al. 2010, p 34).

CFP pipes were placed in the exact same cells as the original high hydraulic conductivity cells. The conductivity values in the high hydraulic conductivity cells were then lowered to match the values of the surrounding hydraulic conductivity cells. Figure 26 shows the network of CFP pipes. The pipe network consists of 1083 pipe nodes and 1087 pipe segments. The pipes in the CFP model were subdivided into pipe network groups based on prominent recharge or discharge points such as sinks or springs. Water temperature is 20.5 degrees Celsius. This value was calculated by averaging the daily temperature measurements from water meters installed in the Wakulla cave system. For the purpose of this model, caves were assumed to occur at the horizontal and vertical center of the model cells, therefore pipe nodes were assigned to the center of the cells which they occupied. Actual measured cave diameter values were only available for caves within the Wakulla Cave System, measured by cave divers from the Global Underwater Explorers organization. Figure 27 shows the Wakulla Spring CFP pipe network group, which represents the Wakulla Cave System. The Wakulla pipe network group has been subdivided into pipe sections based on measured cave diameters. The names of the pipe sections are based on the names given to the caves by the cave divers. A cave diameter data set was provided by Todd Kincaid of Geohydros, Inc. and Casey Mckinlay of Global Underwater Explorers (Todd Kincaid and Casey Mckinlay, written communications, Spring 2010) These diameters were assigned to the CFP pipes that corresponded with the mapped caves. For example, if Cave (or Tunnel) A-1 had a diameter of 50 ft, the value of 50 ft was assigned to Pipe Section A-1. All other diameters for pipes that are not part of the Wakulla pipe network group were estimated during calibration or estimated based on the available field data, which was either provided by Hal Davis of the USGS, or downloaded from the Geohydros, Inc. website (http://www.geohydros.com/FGS/Meters). Tortuosity was calculated for each major cave segment (e.g. Tunnel A, Tunnel R, etc.) mapped by the cave divers. Calculations were done using ArcGIS. Based on these tortuosity measurements in ArcGIS, an average tortuosity value of 1.6 was calculated and applied to all the pipes in the CFP model. The mean height of the pipe wall micro-topography is 0.10. The lower Reynolds number coefficient is 2000.0 and the upper Reynolds number coefficient is 8000.0. Three pipe nodes were set as constant pipe node heads. These three pipe nodes represented the three major springs: Wakulla Spring, Spring Creek Springs Group, and St. Marks Spring. The Wakulla Spring pipe node is set to 5.0 ft, the Spring Creek Springs Group pipe node is set to 0.0 ft, and the St. Marks Spring is set to 9.0 ft. Pipe wall permeability values were initially set equal to hydraulic conductivity values of two orders of magnitude less than the surrounding matrix cells. For example if a pipe node was located in a matrix cell with a hydraulic conductivity of 500 ft/day, the pipe node was assigned a wall permeability value of 5 ft/day.

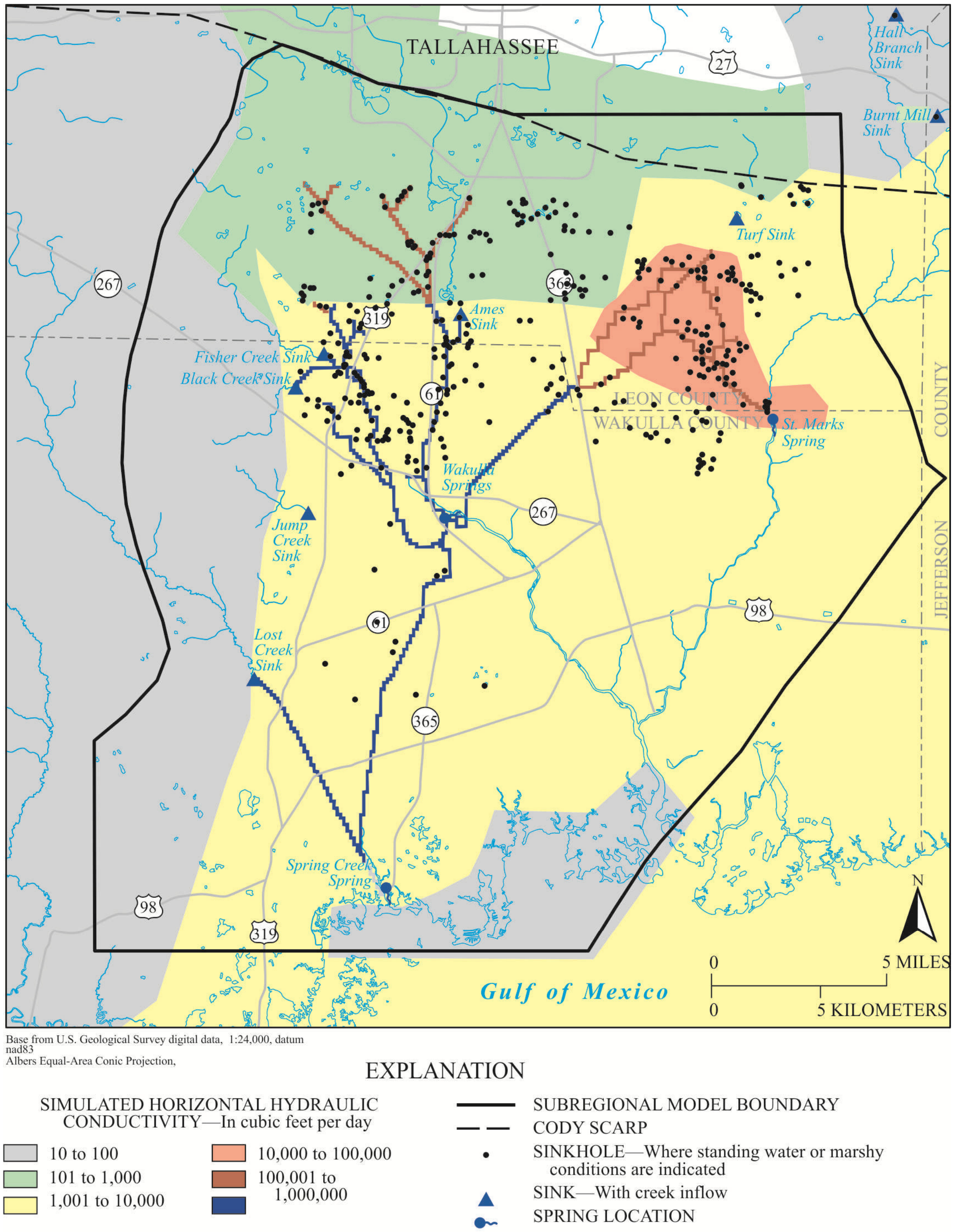

Figure 25: Hydraulic Conductivity of Layer 2 from the MODFLOW-2000 model. The cells in blue and brown are very high hydraulic conductivity cells and represent known and assumed cave locations within the Woodville Karst Plain. It is within these cells that pipe nodes were placed within the CFP model. Sinkhole locations from the surface are present to show how some cave cells were created by Davis et al. (2010) based on the presence of high numbers of sinkholes. Figure from Davis et al. (2010).

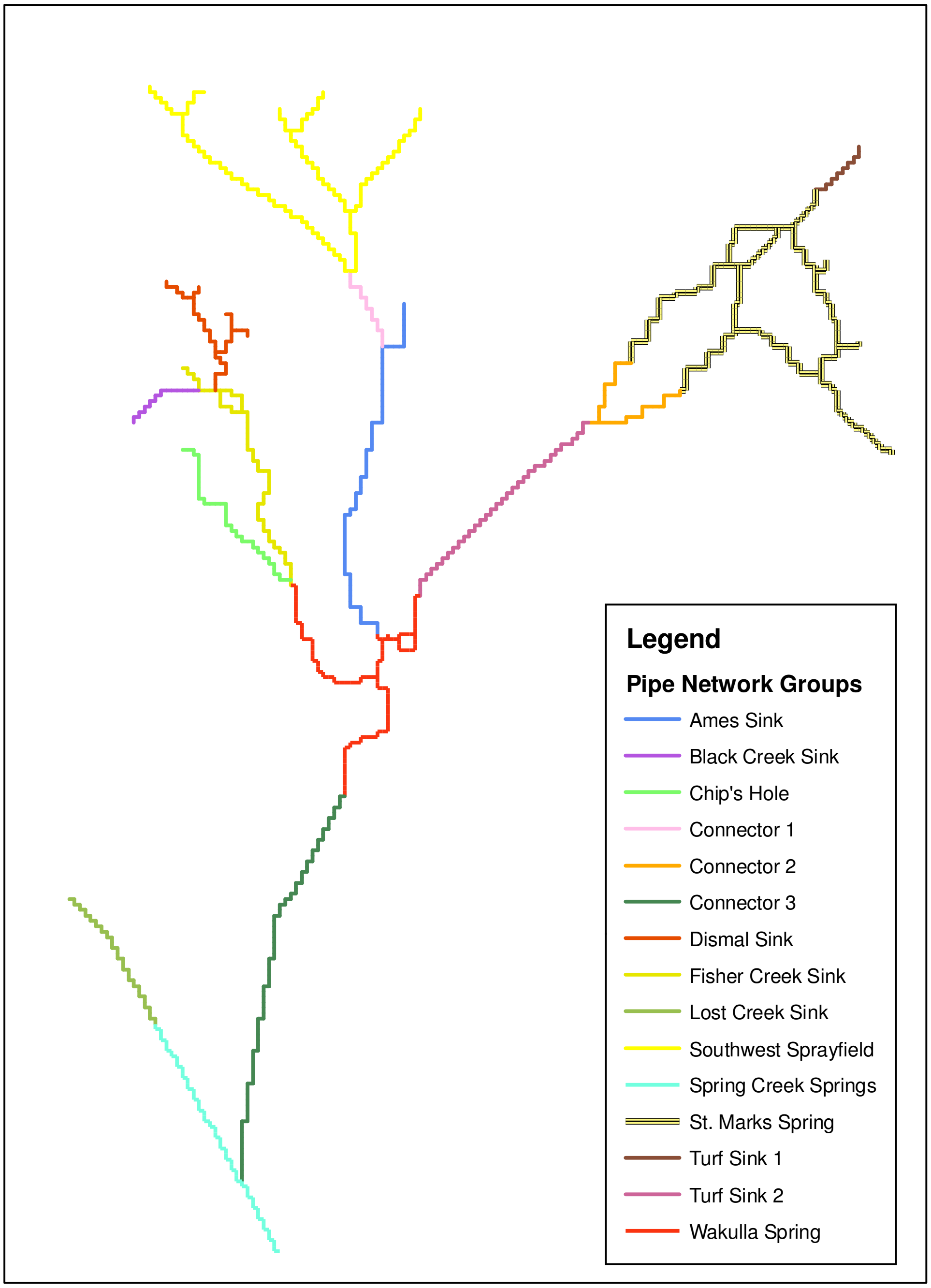

Figure 26: CFP pipe network. This figure shows the CFP pipe network that replaced the very high hydraulic conductivity cells in the MODFLOW-2000 model by Davis et al. (2010). The pipes are separated into pipe network groups based on prominent recharge points (e.g. Fisher Creek Sink) or prominent discharge points (e.g. Wakulla Spring). The Wakulla Spring pipe network group represents the physical Wakulla Springs Cave system, where cave parameters such as cave diameter have been measured.

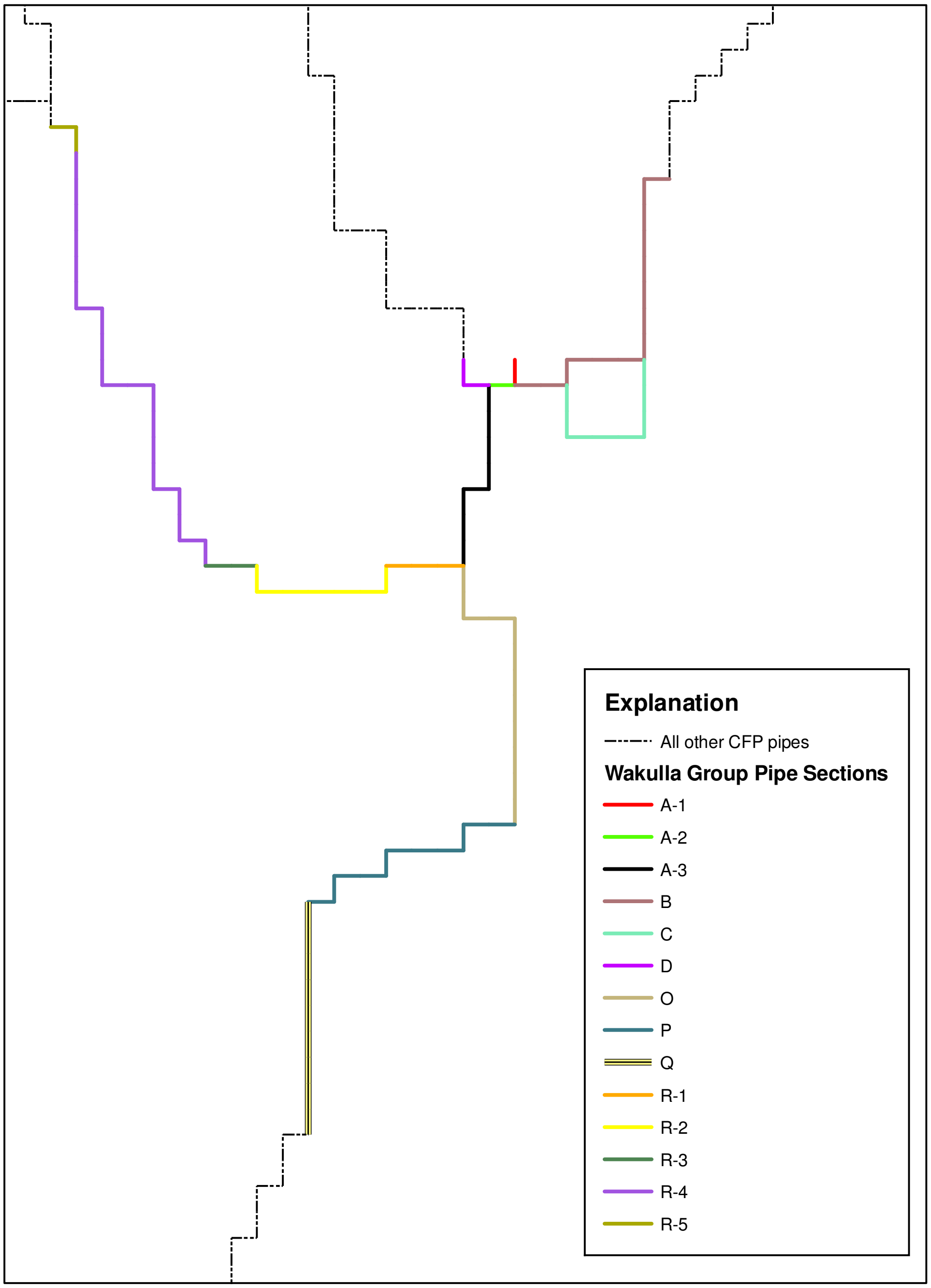

Figure 27: Wakulla Spring CFP Pipe Network Group. This figure shows the Wakulla Spring CFP Pipe Network Group which is subdivided into pipe sections. These pipe sections correspond to the portions of the Wakulla Spring Cave system where pipe diameter has been measured.

4.2.5 Model Calibration

The CFP sub-regional model was calibrated in three steps, using three different data sets: a 1991 USGS head and discharge data set, a 2006 USGS head and discharge data set, and a groundwater tracer study data set from Todd Kincaid of Geohydros (formerly Hazlett-Kincaid). All three data sets were the same data sets used by Davis et al. (2010) to calibrate their sub-regional model. The trial and error method was used to calibrate the CFP model; calibration was done under steady state conditions. Pipe diameter and wall permeability were the only parameters that were varied during calibration of the CFP model. The tortuosity, pipe wall roughness, and Reynolds number values were assumed to be constant. See section 4.2.4 for tortuosity, pipe wall roughness, and Reynolds number values. During calibration, values of pipe diameters and wall permeability were varied by pipe network group or pipe section. For example, all the pipes in the Ames Sink pipe network group were initially set to a pipe diameter of 10 ft. As the model was calibrated, the diameter values of all the pipes within that pipe network group were changed together until a final calibrated value of 30 ft was determined. Appendix B shows the calibrated pipe parameters for the pipes shown in Figure 26 and Figure 27. Since tortuosity, wall roughness, and Reynolds numbers were held constant, those parameters are not shown in the table found in Appendix B. Copies of the input files are in Appendix C.

For the sake of time and simplicity it was decided to use the calibrated hydraulic conductivity values of the MODFLOW cells from Davis et al. (2010). Therefore, cell hydraulic conductivity was not calibrated, but held as a constant. The same calibration criterions of ± 5 ft for head values, ± 10 ft for Wakulla Spring and Spring Creek Springs Group Discharges, and ± 15 ft for St Marks Spring Discharge used by Davis et al. (2010), was used for calibration of the CFP model. These calibration criteria are based on USGS standards for discharge measurements, described on the website http://wdr.water.usgs.gov/current/documentation.html#stage and on page 79 in the USGS Techniques and Methods publication by Turnipseed and Sauer (2010). For the 1991 data set, all discharge into sinkholes was turned off. Constant pipe node heads for Wakulla Spring, Spring Creek Springs Group, and St Marks Spring were set to 5 ft , 0ft , and 9 ft respectively. These head values are yearly averages for the three spring, respectively. For the 2006 data set, all discharges into sinkholes were turned on. Constant pipe node heads for Wakulla Spring, Spring Creek Springs Group, and St Marks Spring were set to 5 ft , 9.5ft , and 9 ft respectively. The head at Spring Creek Springs Group was increased to 9.5 ft to simulate conditions at Spring Creek in 2006 where discharge stopped, and water began flowing northward from Spring Creek to Wakulla Spring. For the tracer test data set, discharges into sinkholes were left on. Constant pipe node heads for Wakulla Spring, Spring Creek Springs Group, and St Marks Spring were set to 5 ft , 0 ft, and 9 ft respectively.

Figure 28a shows the locations of the water wells. Figure 28b shows the simulated and observed water levels for the 1991 data set. For the simulated hydraulic heads, 12 out of 13 hydraulic heads were within the calibration criterion. Figure 29 shows the observed vs. model residual graph. The residual mean is 1.79 ft with a residual standard deviation of 4.44 ft. Residuals tend to plot as positive indicating a possible bias in the model. A spatial analysis of the residuals (Figure 30) also shows this bias, with positive residuals tending to occur along the boundaries of the model, where the model simulation underestimates the observed head values. A very large positive residual exists at the western boundary. This is caused by a problematic well that is located in an area where the hydraulic gradient is very steep. Regarding spring discharges, all three springs were within their respective calibration criterions (Table 3).

For the 2006 data set, Figure 31 shows the simulated and observed water levels. For the simulated heads, 12 out of 97 head measurements were within the calibration criterion. Figure 32 shows the observed vs. residual graph. The residual mean is 1.69 ft with a standard deviation of 2.90 ft. A definite linear bias is observed, indicating bias in the model, with many of the residuals plotting as positive values. The high number of positive residuals indicates that the CFP model underestimates the actual observed head values. A spatial analysis of the 2006 data set residuals (Figure 33) also shows this model bias. Large positive residuals tend to occur within the area of the Tallahassee Sprayfields (northeast corner) and again near the western boundary. Wakulla and St. Marks springs were both within their respective calibration criterion (Table 3). Spring Creek Springs Group does not have a value here because in the 2006 simulation, water began to flow from Spring Creek north to Wakulla. Therefore no discharge was occurring at Spring Creek.

For the Tracer test data set, the model was calibrated until a close match of the simulation to observed tracer travel times was reached. Three tracer tests were used to calibrate the model. The tracer test performed at Ames Sink had a measured residence time of about 20 days. The tracer test performed at Fisher Sink had a measured residence time of about 10 days. The tracer test performed at Turf Sink had a measured residence time of about 40 days (Davis et al. 2010).

Dyes from all three tracer tests exited at Wakulla Spring. While a chemical transport simulation option does not currently exist for CFP mode 1, CFP does calculate the residence time of water within each pipe segment. Residence time is the time it takes for water to travel from the beginning of the pipe to the end of a pipe, and can be assumed to act as a proxy for tracer test travel times. Thus, tracer tests can be simulated by calculating the total amount of time it takes for water to travel through a pipe network from an input point to an output point (i.e. total residence time). For example, to simulate the tracer test performed at Fisher Sink (which exited at Wakulla Spring), the total residence time of the pipe network connected from Fisher Sink to Wakulla Spring was calculated. Pipe diameters were adjusted in the CFP model until a close match to the observed tracer test travel times was achieved. The closest matching simulated residence times were 20.30 days for Ames Sink, 15.83 days for Fisher Sink, and 41.04 days for Turf Sink.

a.)

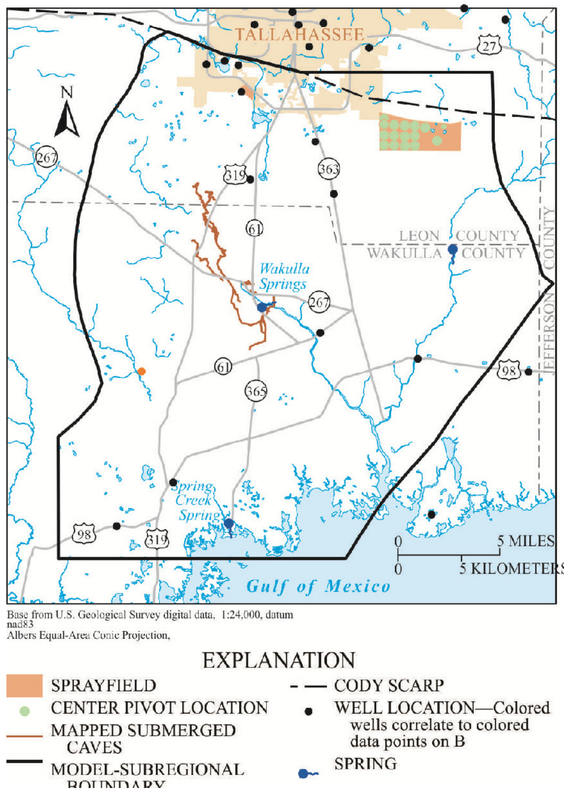

b.)

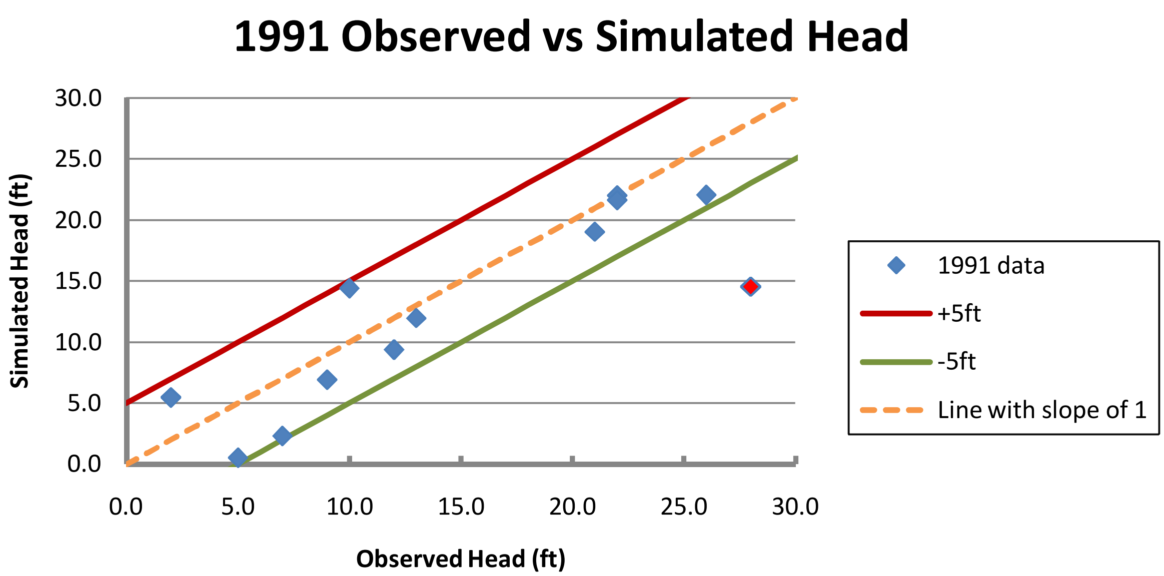

Figure 28: 1991 Observed Head vs. Simulated Head Graph. a.) Map of measured wells for the 1991 data; b.) Observed vs. Simulated head graph showing that all but one of the data points fall within the calibration criterion of ± 5ft. Note that the red data point corresponds to the well (also marked in red) on the southwest side of the karst plain shown in Figure 28a.

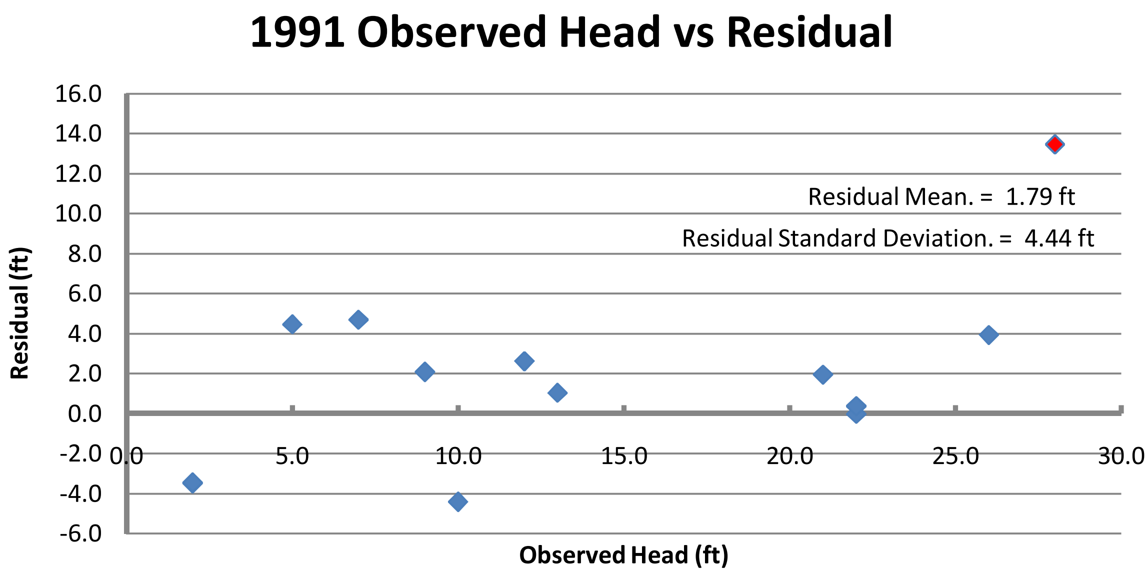

Figure 29: 1991 Observed Head vs. Residual Graph. Much of the data plots above the x-axis line, indicating that there is bias present within the model. The red data point corresponds to the well (also marked in red) on the southwest side of the karst plain shown in Figure 28a.

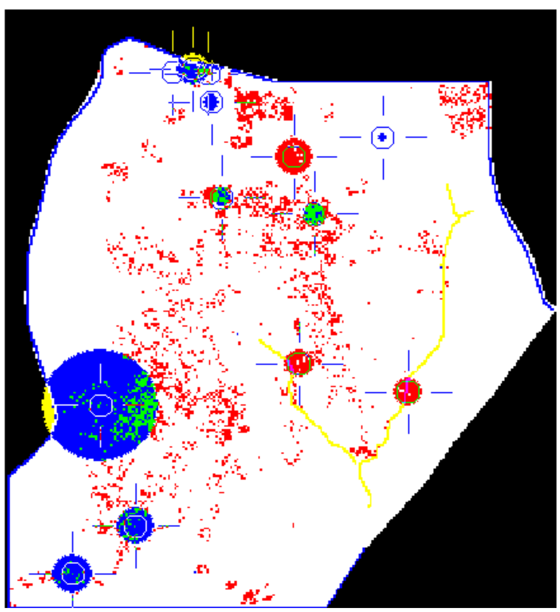

Figure 30: 1991 Spatial Residual Analysis. Target icons represent 1991 wells. Blue circles within the target icons represent positive residuals, while red circles within the targets represent negative residuals. Note that a very large positive residual occurs at the well that is located on the southwest corner of the model, where there is a very steep hydraulic gradient. This is the red well shown in Figure 28a.

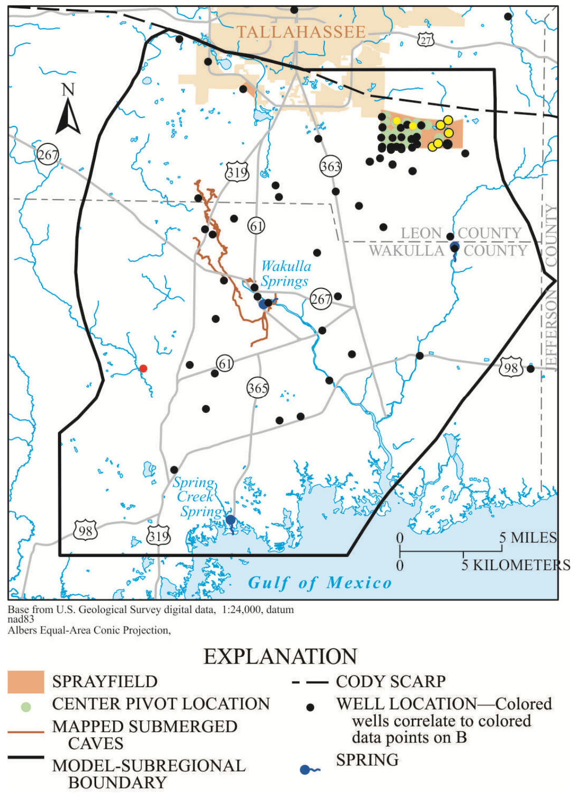

a.)

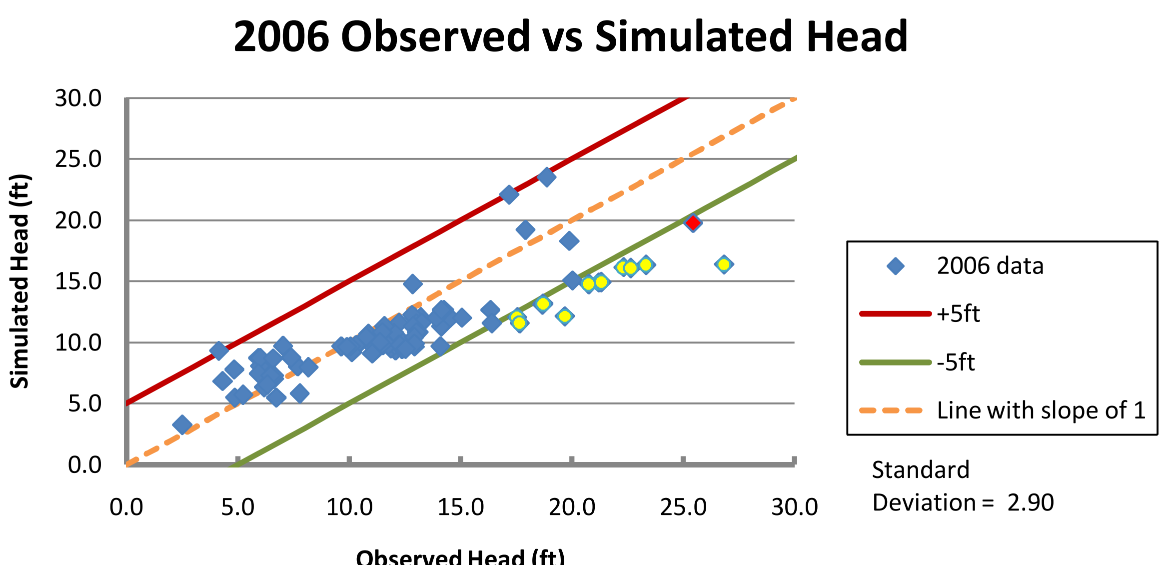

b.)

Figure 31: 2006 Observed Head vs. Simulated Head Graph. a.) Map of measured wells for the 2006 data; b.) Observed vs. Simulated head graph showing that 11 data points fall outside the calibration criterion of ± 5ft. Note that the red data point corresponds to the well (also marked in red) on the southwest side of the karst plain, and the yellow data points correspond to the yellow Sprayfield wells shown in Figure 31a.

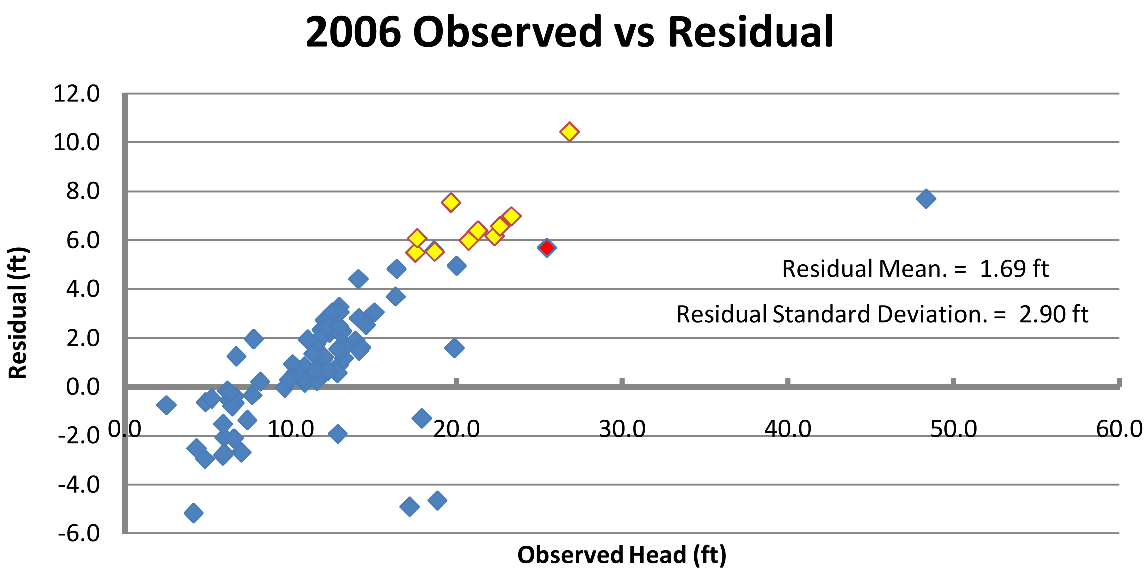

Figure 32: 2006 Observed Head vs. Residual Graph. The linear trend indicates a bias present within the model. The red data point corresponds to the well (also marked in red) on the southwest side of the karst plain and the yellow data points correspond to the yellow Sprayfield wells shown in Figure 31a.

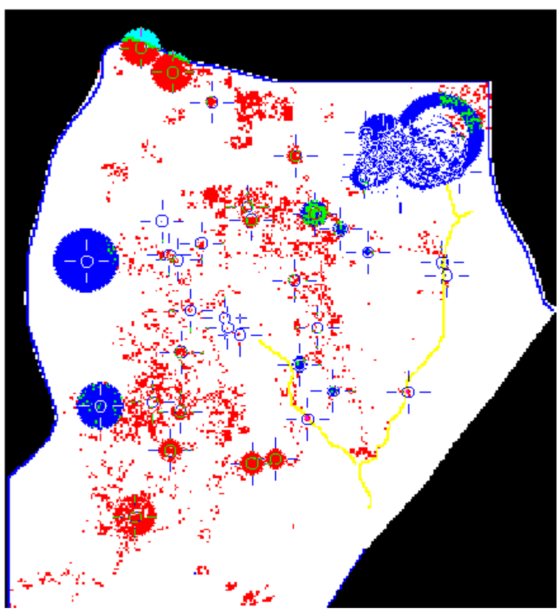

Figure 33: 2006 Spatial Residual Analysis. Blue target icons represent 2006 wells. Blue circles within the target icons represent positive residuals, while red circles within the targets represent negative residuals. Note that very large positive residuals occurs at the well that is located on the southwest corner of the model (corresponding to the red well shown in 31a) where there is a very steep hydraulic gradient and at the wells in the northeast corner of the model (corresponding to the yellow wells in Figure 31a), where the northeast sprayfield is located.

Table 3: Calibrated Simulated Discharges for the Sub-regional Model. a.) Table showing measured and simulated spring discharges for the three major springs for the year 1991; b.) Table showing measured and simulated spring discharges for the three major springs for the year 2006. The symbol cfs stands for cubic feet per second, while cfd stands for cubic feet per day. Note that both tables also show the calculated percent difference between measured and simulated, and the calibration criterion for each spring.

a.)

Spring	1991 Measured Discharge (cfs)	1991 Simulated Discharge (cfd)	1991 Simulated Discharge (cfs)	% Difference	Calibration Criterion (%)
Wakulla	350	32291027.17	373.74	6.8	10
Spring Creek Group	307	25109383.7	290.62	-5.3	10
St Marks	602	49103050.58	568.32	-5.6	15

b.)

Spring	2006 Measured Discharge (cfs)	2006 Simulated Discharge (cfd)	2006 Simulated Discharge (cfs)	% Difference	Calibration Criterion (%)
Wakulla	750	60921274.12	705.11	-6.0	10
Spring Creek Group	0	0	0	0.0	10
St Marks	560	50237279.1	581.45	3.8	15

4.2.6 Transient Model Results

After model calibration, a transient simulation of an actual storm event was run in the model. The storm event took place in August 2008, with peak inflow occurring on August 10, 2008, at 9,158,400 ft^3/d. The transient model was set up with 52 stress periods. Each stress period had only one time step, with the time step equaling one day. The transient model simulated conditions from August 13, 2008 to October 3, 2008. Discharges from the three springs in the model are shown in Figures 34. Prior results from the MODFLOW-2000 model by Davis et al. (2010) are shown in the same figure for comparison. Field data for Wakulla Spring and Spring Creek Springs Group are also shown. There was no available field data for St. Marks Spring.

For Wakulla Spring (Figure 34a), both models simulate a peak in discharge that occurs at approximately the same time as the observed peak discharge. The MODFLOW model overestimates the peak discharge of the storm event, while the CFP model underestimates the peak discharge. This underestimation by CFP is probably due to the CFP model accounting for turbulent flow in its discharge calculations. Examination of the overall shapes of both simulated discharge curves shows that the MODFLOW model does a better job than CFP in simulating the observed discharge throughout the entire 52 time steps.

For Spring Creek Springs Group (Figure 34b), both models do a fairly good job at simulating the overall shape of the observed discharge for the entire 52 time steps. The MODFLOW model underestimates the peak discharge of the storm event, while the CFP model overestimates the peak discharge. Regarding the timing of the peak discharge, the CFP model peak discharge occurs at approximately the same time as the observed discharge. The MODFLOW model simulates a peak discharge that occurs slightly later than what was observed in the field. For St. Marks Spring (Figure 34c), there was no available observed discharge data for the spring. However, comparing the two simulations to each other, both roughly have the same shape, with a peak in discharge, followed by a quick decrease in discharge. The CFP model has a substantially higher peak in discharge than the MODFLOW model.

For each spring, the percent error in peak discharge was calculated to measure the difference in simulated peak discharge with respect to the actual observed peak discharge. For Wakulla Spring, the error percentage of the CFP simulated peak discharge with respect to the field data is -30.1%. Error Percentage of the MODFLOW model with respect to the field data was 30.5%. For Spring Creek Springs, the error percentage of the CFP simulated peak discharge with respect to the field data is 75.8%. Error Percentage of the MODFLOW model with respect to the field data was 42.2%. A percent error calculation was not done for St. Marks Spring since there was no available field data.

For each spring, a percent error for total spring discharge over the 52 time steps was also calculated to measure the difference in total simulated discharge with respect to the total observed discharge. For Wakulla Spring, the error percentage of the total discharge simulated by the CFP model is 0.01%. Error Percentage of the total discharge simulated by the MODFLOW model is 23.2%. For Spring Creek Springs, the error percentage of the total discharge simulated by the CFP model is 21.6%. Error Percentage of the total discharge simulated by the

MODFLOW model is 40.8%. A percent error calculation was not done for St. Marks Spring since there was no available field data. Percent error calculations are shown in Tables 4. Based on these calculations, the MODFLOW model more accurately simulates peak discharge at the springs. However, for the overall 52 time steps of the simulation, CFP simulates the total discharges for each spring more accurately than MODFLOW.

Table 4: Percent Error for the Transient Storm Event Simulation. a.) Percent Error for Wakulla Spring; b.) Percent error for Spring Creek Springs.

a.)

Model	% Error of Peak Discharge	% Error of Total Discharge
CFP	-30.1%	0.01%
MODFLOW	30.5%	23.2%

b.)

Model	% Error of Peak Discharge	% Error of Total Discharge
CFP	75.8%	21.6%
MODFLOW	42.2%	40.8%

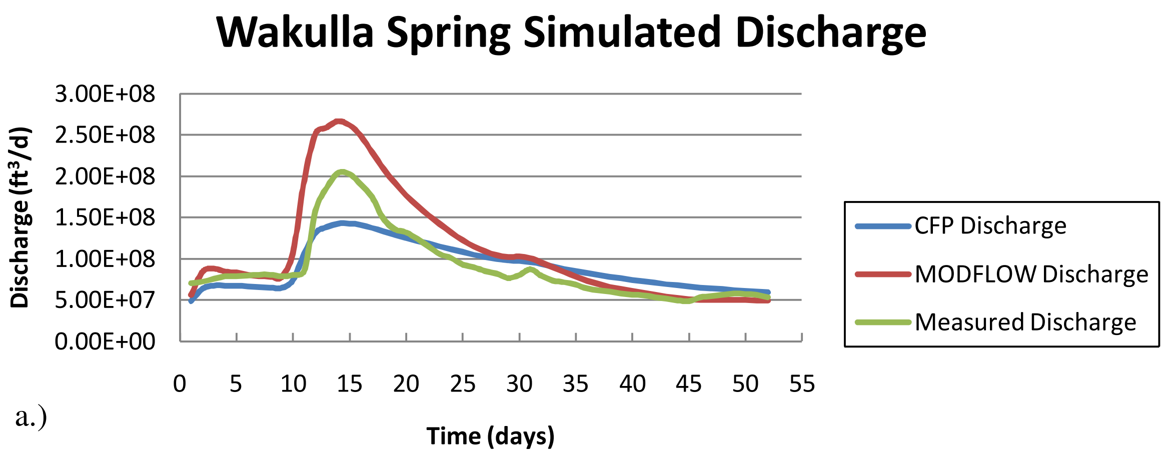

a.)

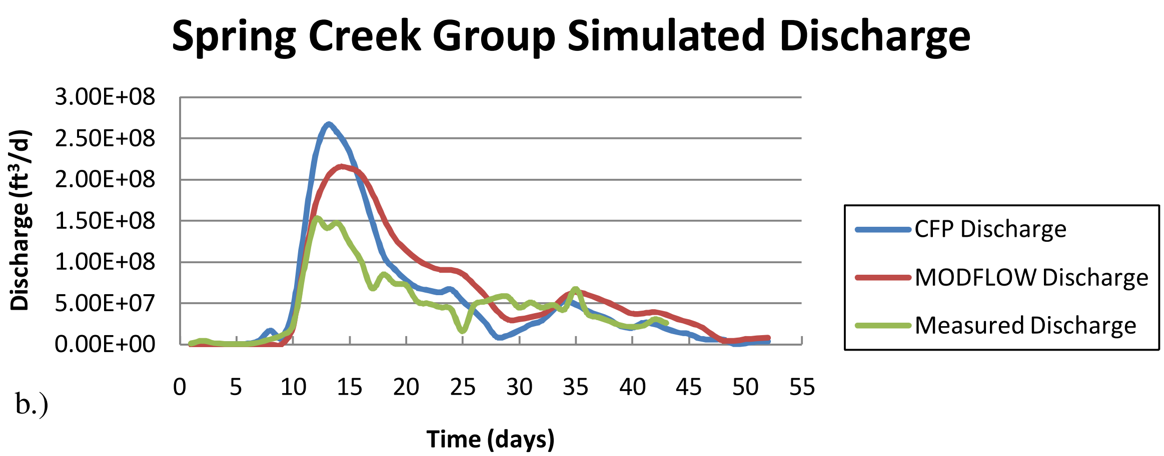

b.)

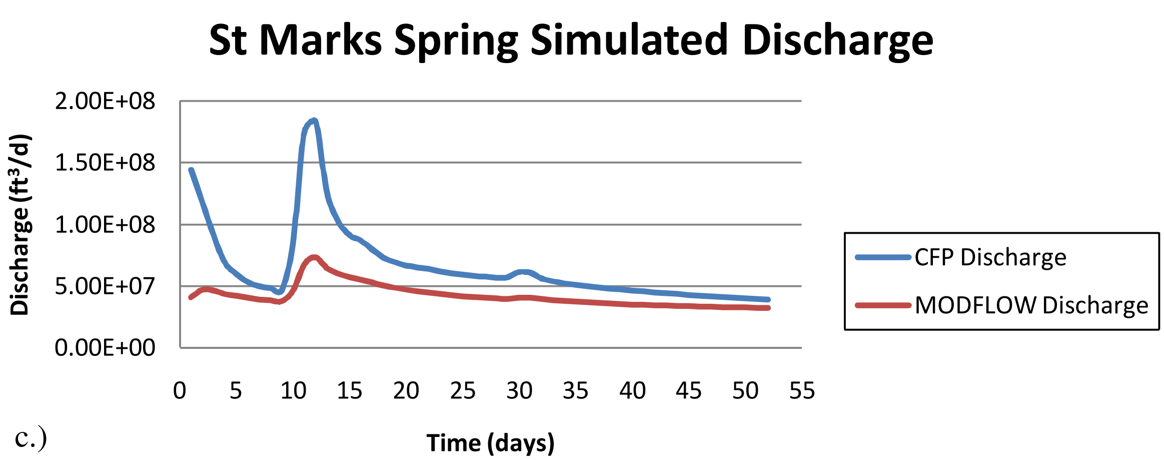

c.)

Figure 34: Spring discharges for the 3 major springs in the model.

4.2.7 Sensitivity Study Results

A sensitivity study of the CFP model was done to further examine the effects of including pipes within a flow model. Four pipe parameters were modified from their calibrated values: pipe diameter, mean height of the pipe walls (i.e. wall roughness), tortuosity, and pipe wall permeability. Results from the sensitivity study are shown below in Figures 35 - 36 for each spring. Each figure shows the amount that a specific model parameter was changed relative to the original calibrated value in units of percent, versus the resulting percent change in spring discharge.

In the sensitivity study, increasing the pipe diameters resulted in an increase in spring discharge for Wakulla Spring and the Spring Creek Springs Group but caused a decrease in the discharge at St. Marks spring (Figure 35a). Decreasing the pipe diameters caused a decrease in discharge for Wakulla Spring and the Spring Creek Springs Group but caused the discharge at St. Marks Spring to increase then decrease. Increasing the roughness of the pipe wall increased discharge at St. Marks spring but decreased discharge at the two other springs (Figure 35b). Decreasing roughness resulted in an increase in discharge at Wakulla Springs and Spring Creek Springs Group, but caused a decrease in discharge at St Marks Spring. A similar effect was seen when tortuosity was increased and then decreased (Figure 36a). Increasing pipe wall permeability resulted in an increase of discharge at all three springs (Figure 36b). Decreasing pipe wall permeability resulted in a decrease of discharge at all three springs.

Figure 37 shows the overall sensitivity of all parameters for each spring with respect to discharge. For all three springs, the most sensitive parameter is pipe diameter. For Wakulla Spring (Figure 37a), pipe wall permeability is the second most sensitive parameter, tortuosity is the third most sensitive, and pipe mean wall height (i.e. roughness) is the least sensitive of the pipe parameters. For Spring Creek Springs Group (Figure 37b), tortuosity is the second most sensitive parameter, mean wall height is the third most sensitive, and wall permeability is the least sensitive parameter. For St Marks Spring (Figure 37c), tortuosity is the second most sensitive parameter, wall permeability is the third most sensitive, and mean wall height is the least sensitive parameter. Overall however, discharge in the model is not very sensitive to tortuosity, wall permeability, or mean wall height.

As previously mentioned above in section 4.2.5, results from three tracer tests were used to help calibrate the CFP model. Using the calibrated residence times based on the three tracer test travel times, a second sensitivity study was done to examine the effects of pipe parameters on groundwater residence time. Results from the sensitivity study are shown below in Figures 38 – 39 for each simulated tracer test. Each figure shows the amount that a specific model parameter was changed relative to the original calibrated value in units of percent, versus the resulting percent change in residence time. For all three simulated tracer tests, increasing the pipe diameter resulted in an increase of residence time, while decreasing the pipe diameter caused a decrease of residence time (Figure 38a). For pipe roughness, the Fisher Creek tracer test showed the most sensitivity to changes in pipe wall roughness, with decreasing residence times when roughness was increased and increasing residence times when roughness was decreased (Figure 38b). Roughness had very little impact on residence time for the Ames Sink and Turf Sink tracer test. For tortuosity, residence time increased slightly for all three tracer tests when tortuosity was increased (Figure 39a). When tortuosity was decreased, the Ames Sink and Turf Sink tracer test residence times decreased slightly while the residence time of the Fisher Sink tracer test greatly increased. For pipe wall permeability, increasing the wall permeability increased residence time, and decreasing the permeability decreased the residence time for the Fisher Sink tracer test (Figure 39b). For the Ames and Turf Sinks Tracer tests, increasing the wall permeability decreased residence time while decreasing the permeability increased the residence time.

Figure 40 shows the overall sensitivity of all parameters for each tracer test with respect to residence time. For all three simulated tracer tests, the most sensitive parameter is pipe diameter. For the Fisher Sink tracer test, tortuosity is the second most sensitive parameter (especially when tortuosity is decreased enough), roughness is the third most sensitive, and pipe wall permeability is the least sensitive of the pipe parameters. For the Ames Sink and Turf Sink tracer tests, wall permeability is the second most sensitive parameter, tortuosity is the third most sensitive, and wall roughness is the least sensitive parameter.

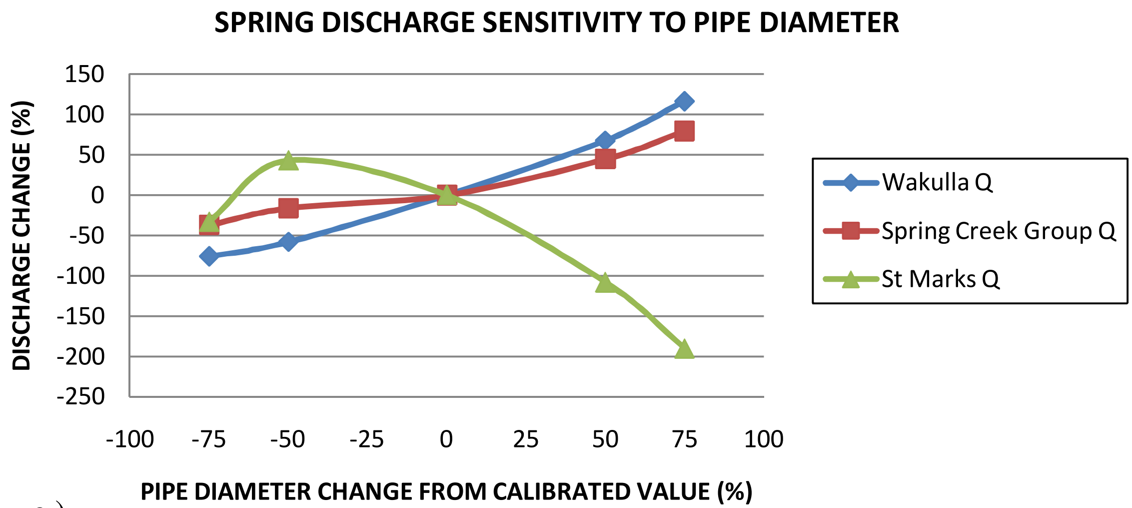

a.)

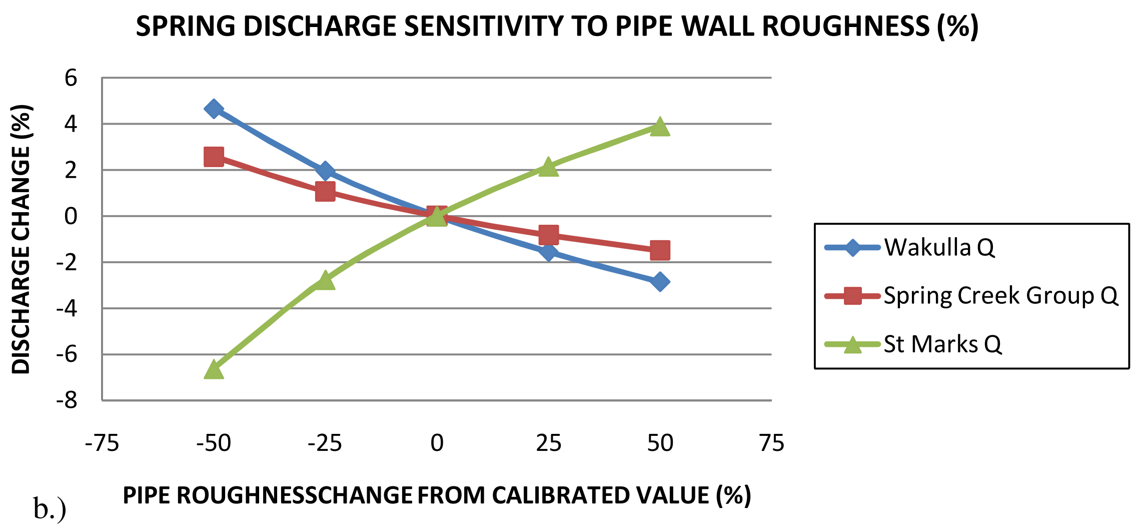

b.)

Figure 35: Discharge sensitivity to pipe diameter and wall roughness. a.) Discharge Sensitivity to pipe diameter; b.) Discharge Sensitivity to Pipe wall roughness

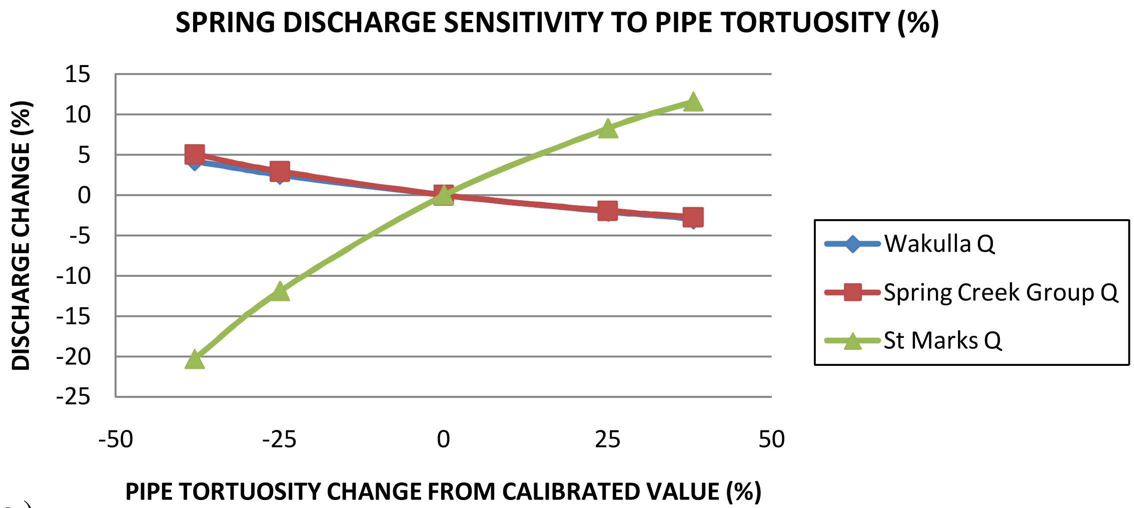

a.)

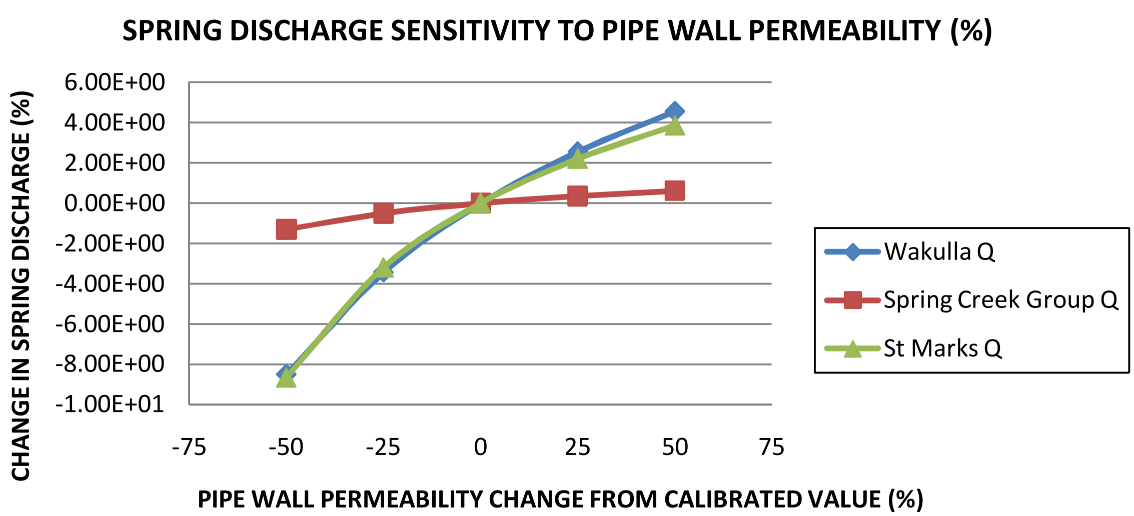

b.)

Figure 36: Discharge Sensitivity to tortuosity and pipe wall permeability. a.) Discharge Sensitivity to tortuosity; b.) Discharge Sensitivity to pipe wall permeability.

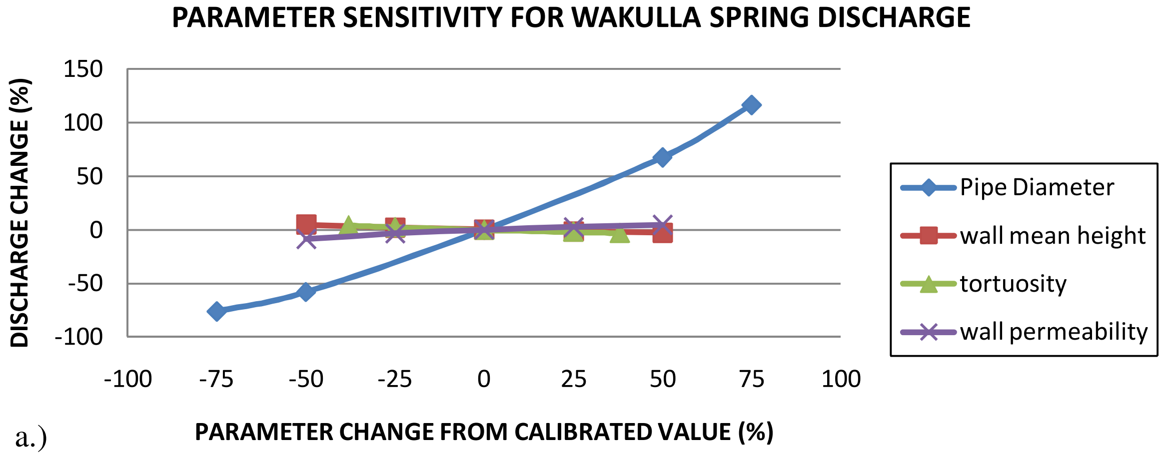

a.)

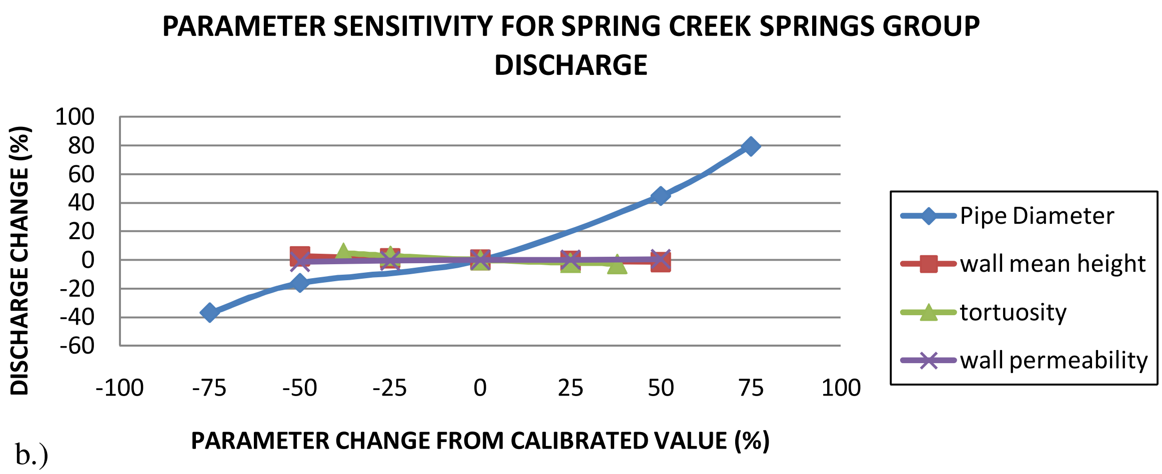

b.)

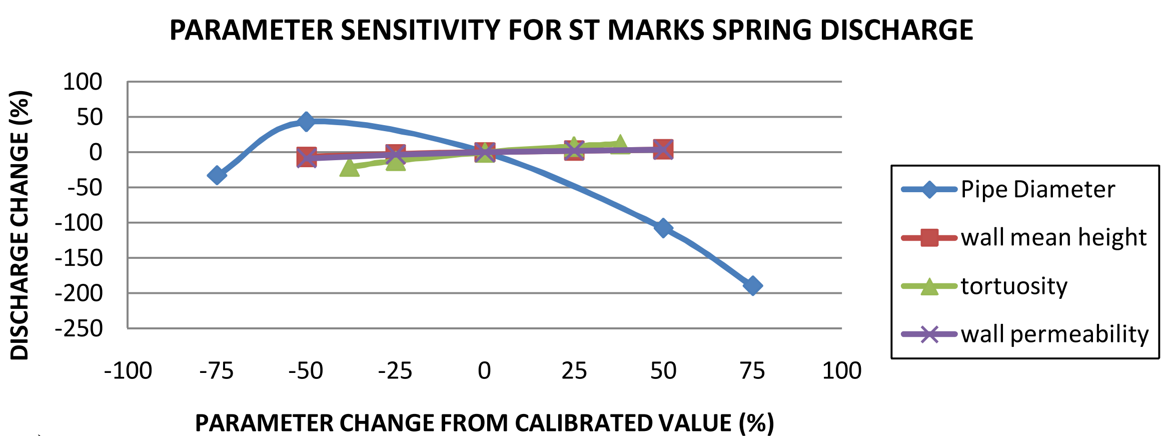

c.)

Figure 37: Overall sensitivity of each spring to all 4 pipe parameters. a.) Wakulla Spring; b.) Spring Creek Springs Group; c.) St. Marks Spring.

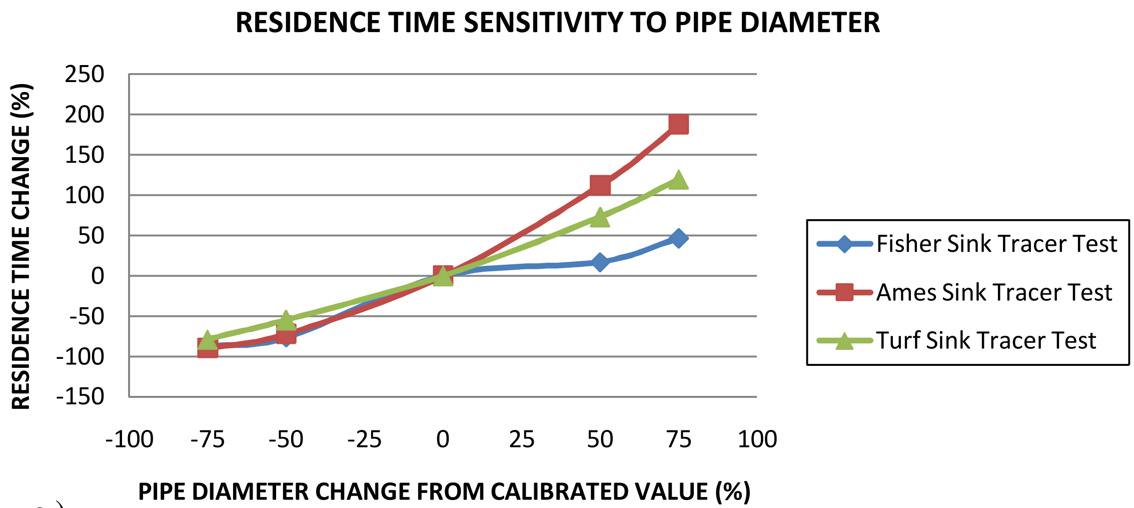

a.)

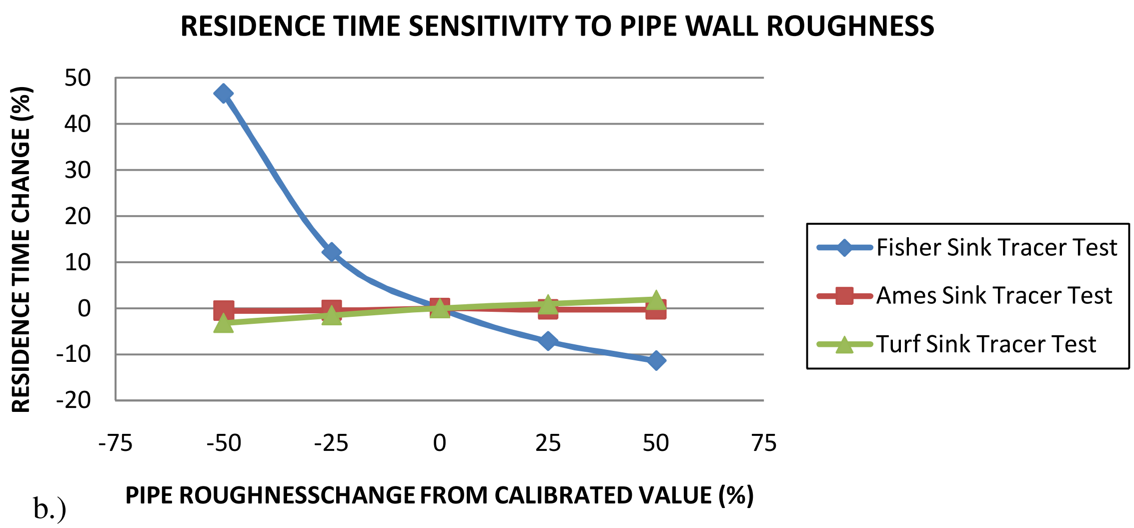

b.)

Figure 38: Residence time sensitivity to pipe diameter and wall roughness. a.) Residence time sensitivity to pipe diameter; b.) Residence time sensitivity to pipe wall roughness.

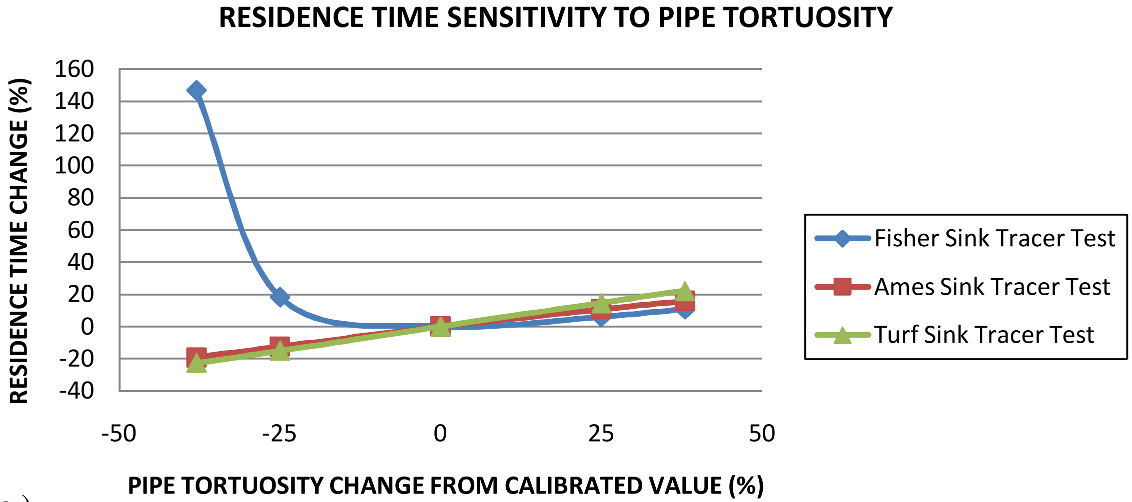

a.)

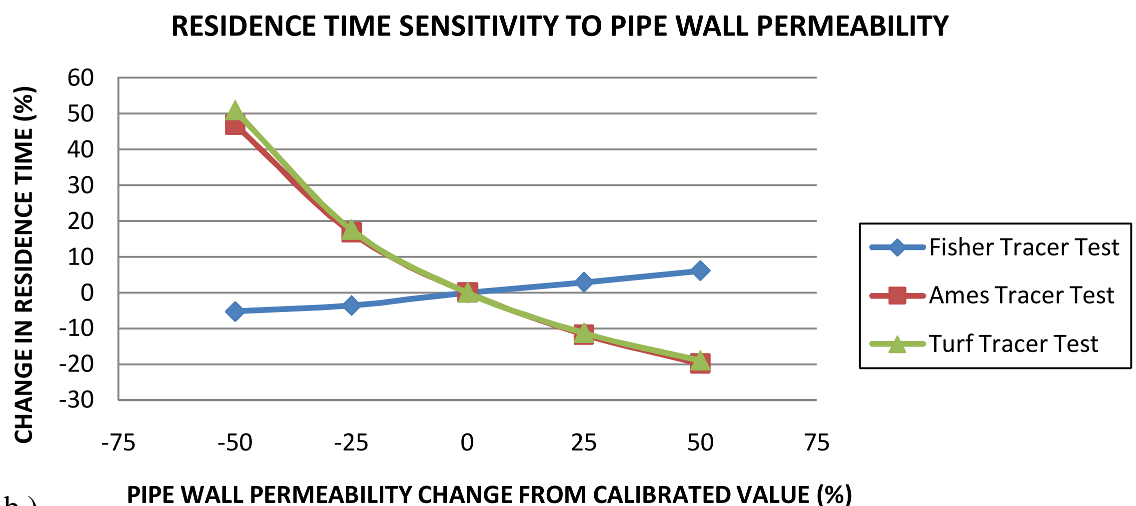

b.)

Figure 39: Residence time sensitivity to tortuosity and wall permeability. a.) Residence time sensitivity to tortuosity; b.) Residence time sensitivity to Pipe wall permeability.

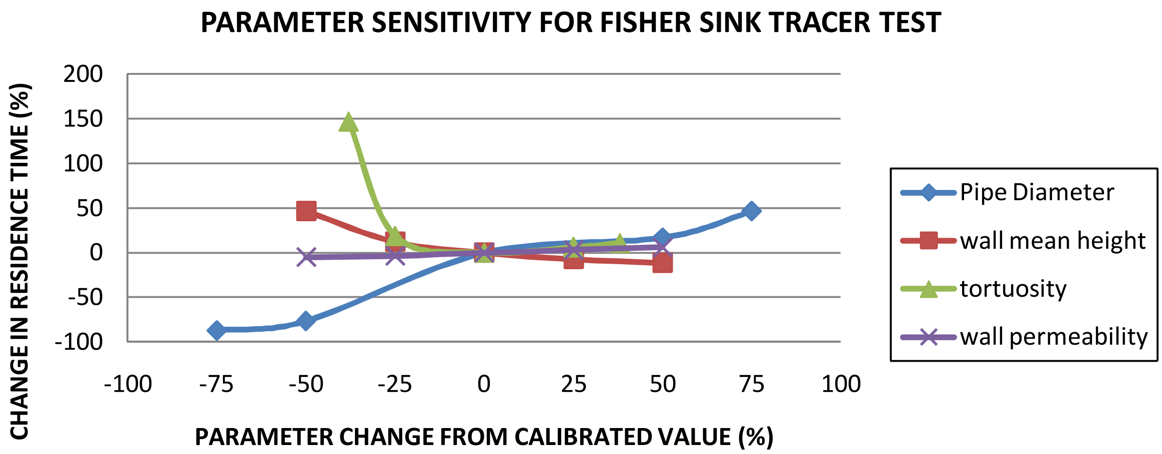

a.)

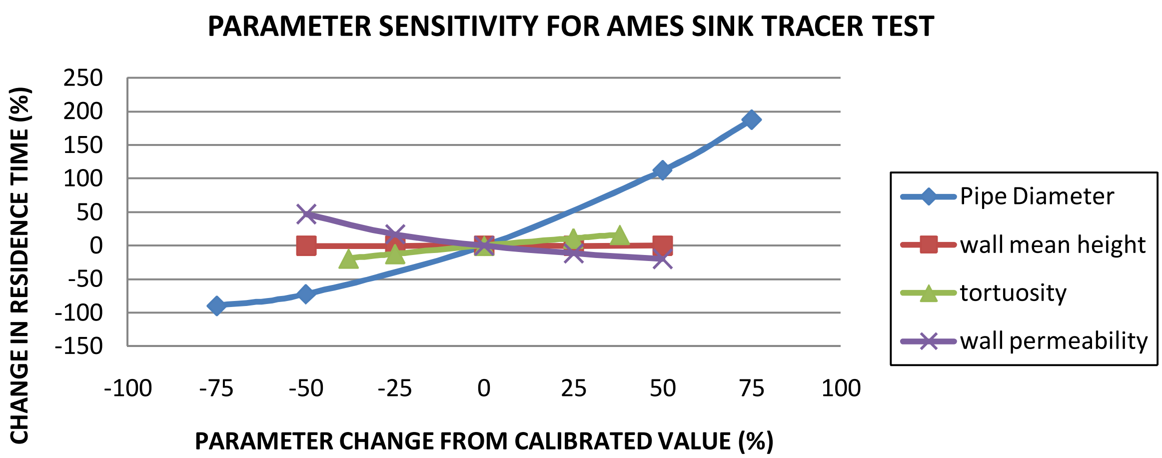

b.)

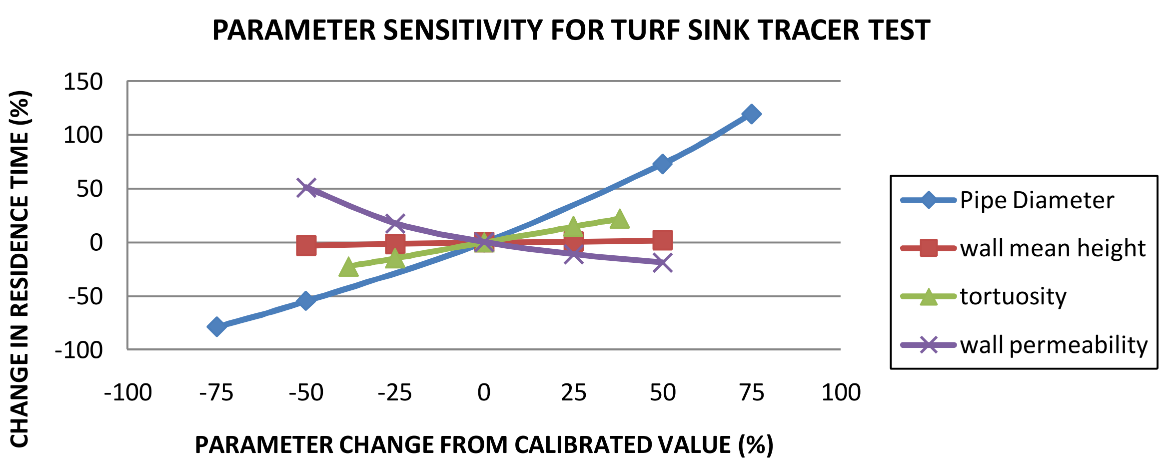

c.)

Figure 40: Overall residence time sensitivity to all 4 pipe parameters. a.) Fisher creek test; b.) Ames Sink Test; c.) Turf Sink Test.

CHAPTER FIVE

CONCLUSION

The purpose of this Thesis was to evaluate the ability of MODFLOW-CFP to accurately simulate flow in karst aquifers. The major hypothesis of this Thesis was that MODFLOW-CFP would more accurately simulate flow in karst aquifers than MODFLOW-2005 (or 2000) because MODFLOW-CFP accounts for turbulent flow, as well as pipe parameters such as pipe diameter, tortuosity, etc. To test this hypothesis, two studies were performed: one at a laboratory scale and another at a sub-regional scale. For the laboratory scale study, a CFP model and a MODFLOW-2005 model were created, based on a laboratory scale karst analog model. Results of the two numerical models were then compared to each other and the original karst model. Results from the laboratory scale model show that the CFP model was more accurate than the MODFLOW-2005 numerical model. For the sub-regional model, a CFP model of the Woodville Karst Plain was created, based on a previous MODFLOW-2000 model. A transient simulation of an actual storm event was then run in both models. Results from both models were compared to observed discharges at Wakulla Spring, Spring Creek Springs Group, and St. Marks Spring. Results from the sub-regional scale study show that the MODFLOW model more accurately simulated the peak discharges of the springs, than did CFP. However, for the overall 52 time steps of the simulation, results show that the CFP model simulated the total discharges for each spring more accurately than MODFLOW.

A sensitivity study of the sub-regional CFP model was also done. The sensitivity study had two parts: the first part tested the sensitivity of discharge with respect to pipe parameters, while the second part tested the sensitivity of residence time within pipes with respect to pipe parameters. Both the discharge and residence time sensitivity studies showed that the pipe diameter of simulated karst features (e.g. caves and conduits) was the most highly sensitive parameter. For the discharge sensitivity study, all other pipe parameters (pipe wall permeability, tortuosity, and roughness) had relatively less impact on discharge. However, for the residence time study, residence time was also sensitive to tortuosity, wall permeability, and roughness, depending on the spring.

Previous studies by others showed that CFP could be used to simulate flow at a laboratory scale (Kuniansky et al., 2008) using CFP mode 2 and at a local scale (Hill et al., 2010) using CFP mode 1. This thesis was the first to attempt an evaluation of CFP at a laboratory and sub-regional scale using CFP mode 1. As previously discussed, results from the laboratory scale study show that using CFP increases accuracy of simulations at the laboratory scale. However at the sub-regional scale results are mixed, with CFP increasing the accuracy of total simulated discharges, yet failing to accurately simulate peak discharges. Based on these results and the results from Hill et al. (2010), CFP can easily increase simulation accuracy for karst groundwater models that are at a scale less than a sub-regional scale. However as this thesis shows, CFP does not yield definitively more accurate results at the sub-regional scale.

The reason for this lies in the use of pipe parameters that one must define within CFP. In a way, CFP is like a two edged sword. On the one hand, the use of CFP can increase accuracy of a simulation, because CFP can create more realistic models. It does this by using pipe equations that account for turbulent flow within karst features, and incorporating into its discharge and head calculations, pipe parameters such as tortuosity, pipe wall roughness, and wall permeability. On the other hand, with the ability to create a more realistic model comes the requirement by CFP to define and use more parameters that are not needed in previous MODFLOW versions. With CFP (mode 1), the user is burdened with the requirement to define many pipe parameters that are not needed in previous MODFLOW versions. At smaller scales, it is easier to determine karst parameters. For example, at the local scale, many of the karst caves and conduits to Wakulla Spring have been mapped, with many parameters, such as diameter and tortuosity, easily measured or reasonably estimated. Thus, at a smaller scale, CFP provides more accurate results because many of the key parameters are available. However at larger scales (e.g. sub-regional), not all caves have been mapped, and all areas are not hydrogeologically well understood; the system is very complex. Thus karst conduit locations and parameters must be guessed, based on many assumptions and inferences. This potentially leads to models producing simulations results that do not match reality very well, such as inaccurately simulated peak discharges. The definitive increase in simulation accuracy by using CFP at a sub-regional scale therefore depends on how well understood the cave system is within the karst aquifer being modeled.

However, the use and importance of CFP should not be discounted. The results of this thesis do not indicate a flaw with CFP, but rather a limitation of CFP based on the complexity of karst. The only reason CFP did not yield a more accurate peak discharge result in the sub-regional study was because not enough cave parameters were known and that the location of several karst caves (e.g. the St. Marks Cave Group) had to be guessed. CFP is still useful for local scale studies, especially for studies that involve fate and transport. As shown by the residence time sensitivity study, pipe parameters such as tortuosity, wall permeability, and even roughness, can affect the amount of time it takes water (and any water borne contaminant) to travel through pipes. CFP can also calculate flow directions within individual pipe networks, a helpful feature when trying to determine contaminant transport.

For future work, this study can be continued by re-evaluating the hydraulic conductivity values of the sub-regional model. Early on in this study it was decided that for the sake of this Thesis, the matrix cells hydraulic conductivities calculated by Davis et al. (2010) and used in their MODFLOW-2000 model, would be assumed to be accurate and used for the matrix cells of the CFP model. However, the matrix cell hydraulic conductivities calculated by Davis et al. (2010) may be inflated (too high) given that Davis et al. were trying to simulate pipe flow using MODFLOW-2000, which is an EPM model that does not account for flow through pipes. These inflated hydraulic conductivities could potentially have contributed to error in the CFP model. Re-calibrating the matrix cell hydraulic conductivities could potentially fix the error with the CFP simulated peak discharges. Work on this study can also be continued by using a program such as UCODE to automatically calibrate the CFP model, in an effort to increase the accuracy of the CFP model.

In conclusion, the ability of CFP to more accurately simulate karst flow conditions is limited by the availability of pipe parameters and cave location. This thesis shows that at a laboratory scale CFP easily produces more accurate results than MODFLOW. At the sub-regional scale, when considering total discharge over the entire simulation, CFP produces more accurate results than MODFLOW. However, for simulated peak discharges at the sub-regional scale, CFP does not produce more accurate results.

APPENDIX A

MODFLOW-CFP INPUT FILE FOR THE LABORATORY SCALE MODEL

```
#CFP input file for Laboratory Scale Karst Analog Model
#Mode
1
#data for the conduit system
#number of nodes / tubes / layers
10  9  6
#temperature
19.8
#No  mc mr ml Nb1  Nb2  Nb3  Nb4 Nb5  Nb6 tb1 tb2 tb3 tb4 tb5 tb6
1   1  1  6  2   0   0   0  0   0  1  0  0  0  0  0
2   2  1  6  1   3   0   0  0   0  1  2  0  0  0  0
3   3  1  6  2   4   0   0  0   0  2  3  0  0  0  0
4   4  1  6  3   5   0   0  0   0  3  4  0  0  0  0
5   5  1  6  4   6   0   0  0   0  4  5  0  0  0  0
6   6  1  6  5   7   0   0  0   0  5  6  0  0  0  0
7   7  1  6  6   8   0   0  0   0  6  7  0  0  0  0
8   8  1  6  7   9   0   0  0   0  7  8  0  0  0  0
9   9  1  6  8   10  0   0  0   0  8  9  0  0  0  0
10 10  1  6  9   0   0   0  0   0  9  0  0  0  0  0
#Node elevations, Two possibilites
#first: node #, elevation
#second: number of nodes, distance from centroid (only one line)
10 -1.0
#surface dependent exchange (set 1) or constant exchange (set 0)
1
#criterion for convergence
1.0D-6
#maximum number for loop iterations
200
#parameter of relaxation
0.98
#Newton Rhapson Print Flag
1
#data of tube parameters:
#no. diameter  tort     roughness   lcritrey   tcritrey
1    2.0       1.0      0.00001     4000.      12000.
2    2.0       1.0      0.00001     4000.      12000.
3    2.0       1.0      0.00001     4000.      12000.
4    2.0       1.0      0.00001     4000.      12000.
5    2.0       1.0      0.00001     4000.      12000.
6    2.0       1.0      0.00001     4000.      12000.
7    2.0       1.0      0.00001     4000.      12000.
8    2.0       1.0      0.00001     4000.      12000.
9    2.0       1.0      0.00001     4000.      12000.
#node heads (if head unequal -1 the head is fixed)
1   32.51
2   -1
```

3 -1
4 -1
5 -1
6 -1
7 -1
8 -1
9 -1
10 32.49
#wall permeability for flow between continuum and pipe-network
1 0.0619
2 0.0619
3 0.0619
4 0.0619
5 0.0619
6 0.0619
7 0.0619
8 0.0619
9 0.0619
10 0.0619

APPENDIX B

CALIBRATED PIPE PARAMETERS

Table 5: Calibrated Pipe Diameters and Wall Permeabilities for the Sub-regional model. Table is divided into Pipe Groups (see Figure 26). All other pipe parameters were held constant, so are not shown here.

Pipe Group	Pipe Diameter (ft)	Pipe Wall Permeability (ft/day)
Ames Sink	30	15
Black Creek Sink	20	15
Chip’s Hole	15	15
Connector 1	20	15
Connector 2	50	15
Connector 3	10	75
Dismal Sink	20	30
Fisher Creek Sink	15	30
Lost Creek Sink	30-50	950
Southwest Sprayfield	10	5
Spring Creek Springs	50	950
St. Marks Spring	50	300
Turf Sink 1	50	32.5
Turf Sink 2	40	15
Wakulla Spring	See Table 5	See Table 5

Table 6: Calibrated Pipe Diameters and Wall Permeabilities, for the Wakulla Spring Pipe Network Group, divided into Pipe sections (see Figure 27). All other pipe parameters were held constant, so are not shown here.

Pipe Section	Pipe Diameter (ft)	Pipe Wall Permeability (ft/day)
A-1	50	30
A-2	60	30
A-3	50	30
B	10	30
C	10	30
D	10	30
O	25	30
P	50-55	75
Q	10	75
R-1	20	30
R-2	10	30
R-3	25	30
R-4	30	30
R-5	50	30

APPENDIX C

MODFLOW-CFP INPUT FILE FOR THE SUB-REGIONAL SCALE MODEL

Note: The original input file is too large to include in this appendix. Shown below is a condensed version of the input file.

```
#SUBREGIONALWOODVILLE KARST PLAIN CFP MODEL
# MODFLOW2005 CFP Input File – MODE TYPE
 1
#
# NNODES NPIPES NLAYERS
 1083  1087  2
# TEMPERATURE
  20.500000
# Node Number, (R,C,L), 6 nodes numbers, 6 pipe numbers
  1   109 156 2    2 1081 0 0 0 0 1 1085 0 0 0 0
 2   109 157 2    1 3 783 0 0 0 1 2 782 0 0 0
 3   108 157 2    2 4 605 0 0 0 2 3 604 0 0 0
 4   108 158 2    3 5 0 0 0 0 3 4 0 0 0 0
 5   108 159 2    4 6 0 0 0 0 4 5 0 0 0 0
 6   108 160 2    5 7 0 0 0 0 5 6 0 0 0 0
 7   108 161 2    6 8 0 0 0 0 6 7 0 0 0 0
 8   107 161 2    7 9 0 0 0 0 7 8 0 0 0 0
 9   107 162 2    8 10 0 0 0 0 8 9 0 0 0 0
 10   107 163 2    9 11 0 0 0 0 9 10 0 0 0 0
.
.
.
1080   108 102 2    1079 538 0 0 0 0 1083 1084 0 0 0 0
 1081   109 156 1      1 0 0 0 0 0 1085 0 0 0 0 0       <-------Wakulla Vent
 1082    89 270 1    1064 0 0 0 0 0 1086 0 0 0 0 0       <-------Spring Creek Vent
 1083   204 124 1    914 0 0 0 0 0 1087 0 0 0 0 0       <-------St Marks Vent
#
#
# GEOHEIGHT Option 1
 1083  0.000000
#  SA_EXCHANGE
 1
# EPSILON
  1.000000e-002
# NITER
  100
# RELAX
  1.000000
# P_NR
  1
#
# Pipe Diameter Tortuosity RHEIGHT  Lower-Reynolds   Upper-Reynolds
```

```
 1  50.000000 1.600000e+000 0.100000 2000.000000 8000.000000
 2  60.000000 1.600000e+000 0.100000 2000.000000 8000.000000
 3  50.000000 1.600000e+000 0.100000 2000.000000 8000.000000
 4  50.000000 1.600000e+000 0.100000 2000.000000 8000.000000
 5  50.000000 1.600000e+000 0.100000 2000.000000 8000.000000
 6  50.000000 1.600000e+000 0.100000 2000.000000 8000.000000
 7  50.000000 1.600000e+000 0.100000 2000.000000 8000.000000
 8  50.000000 1.600000e+000 0.100000 2000.000000 8000.000000
 9  50.000000 1.600000e+000 0.100000 2000.000000 8000.000000
 10  50.000000 1.600000e+000 0.100000 2000.000000 8000.000000
.
.
.
1084  20.000000 1.600000e+000 0.100000 2000.000000 8000.000000
1085  100.000000 1.600000e+000 0.10000 2000.000000 8000.000000   <---------Wakulla Vent
1086  50.000000 1.600000e+000 0.10000 2000.000000 8000.000000   <-------Spring Creek vent
1087  50.000000 1.600000e+000 0.10000 2000.000000 8000.000000   <------------St Marks vent
# Node  Head
 1  -1.000000
 2  -1.000000
 3  -1.000000
 4  -1.000000
 5  -1.000000
 6  -1.000000
 7  -1.000000
 8  -1.000000
 9  -1.000000
 10  -1.000000
.
.
.
1080  -1.000000
1081  5.000000  <------Wakulla vent
1082  0.000000  <------Spring Creek vent
1083  9.000000  <------St Marks vent
# Node K_EXCHANGE
 1  30.000000
 2  30.000000
 3  30.000000
 4  30.000000
 5  30.000000
 6  30.000000
 7  30.000000
 8  30.000000
 9  30.000000
 10  30.000000
.
.
.
1080  15.000000
1081   5.000000  <-----Wakulla Vent
1082  125.0000000  <-----Spring Creek Vent
1083  50.00000000  <-----St. Marks vent
```

REFERENCES

Anderson, M. P., & Woessner, W. W. (2002). *Applied groundwater modeling : Simulation of flow and advective transport*. San Diego: Academic Press.

Barrios, K., (2006). *St. Marks River and Wakulla River Springs Inventory, Leon and Wakulla Counties, Florida.* Northwest Florida Water Management District, Water Resources Special Report 06-03.

Bauer, S., Liedl, R., & Sauter, M. (2003). Modeling of karst aquifer genesis: Influence of exchange flow. *Water Resources Research, 39*(10).

Berner, R., & Morse, J. (1974). Dissolution kinetics of calcium-carbonate in sea-water. 4.Theory of calcite dissolution. *American Journal of Science, 274*(2), 108-134.

Clemens, T., Huckinghaus, D., Sauter, M., Liedl, R., & Teutsch, G. (1996). A combined continuum and discrete network reactive transport model for the simulation of karst development. *IAHS-AISH Publication,* (237), 309-318.

Davis, J.H., & Katz, B.G. (2007). *Hydrogeologic Investigation, Water Chemistry Analysis, and Model Delineation of contributing Areas for City of Tallahassee Public-Supply Wells, Tallahassee, Florida:* U.S. Geological Survey Scientific Investigations Report 2007-5070, 67 p.

Davis, J.H., & Katz, B.G., & Griffin, D.W. (2010). *Nitrate-N Movement in Groundwater from the Land Application of Treated Municipal Wastewater and Other Sources in the Wakulla Springs Springshed, Leon and Wakulla Counties, Florida, 1966-2018:* U.S. Geological Survey Scientific Investigations Report 2010-5099, 90 p.

DiFrenna, V., Price, R., & Savabi, M. (2008). Identification of a hydrodynamic threshold in karst rocks from the Biscayne aquifer, south Florida, USA. *Hydrogeology Journal, 16*(1), 31-42.

Dreybrodt, W. (1990). The role of dissolution kinetics in the development of karst aquifers in limestone – a model simulation of karst evolution. *The Journal of Geology, 98*(5), 639-655.

Faulkner, J. (2008). *Laboratory analog study of groundwater flow and solute transport in a karst aquifer with conduit and matrix domains* (Master’s thesis). Florida State University, Tallahassee, Florida.

Faulkner, J., Hu, B., Kish, S., & Hua, F. (2009). Laboratory analog and numerical study of groundwater flow and solute transport in a karst aquifer with conduit and matrix domains. *Journal of Contaminant Hydrology, 110*(1-2), 34-44.

Fetter, C. W. (2001). *Applied hydrogeology* (4^{th} ed.). Upper Saddle River, N.J.: Prentice Hall.

Ford, D., & Williams, P. W. (2007). *Karst hydrogeology and geomorphology* (Rev ed.). Chichester, England ; a Hoboken, NJ: John Wiley & Sons.

Freeze, R. A., Cherry, J. A., & Cherry, J. A. (1979). *Groundwater*. Englewood Cliffs, N.J.: Prentice-Hall.

Harbaugh, A.W., Banta, E.R., Hill, M.C., and McDonald, M.G. (2000). *MODFLOW-2000, the U.S. Geological Survey modular ground-water model – user guide to modularization concepts and the Ground-Water Flow Process*: U.S. geological Survey Open-File Report 00-92, 121 p.

Hill, M., Stewart, M., & Martin, A. (2010). Evaluation of the MODFLOW-2005 conduit flow process. *Ground Water, 48*(4), 549-559.

Hornberger, G. M., Raffensperger, J. P., Wiberg, P. L., & Eshleman, K. N. (1998). *Elements of physical hydrology*. Baltimore: Johns Hopkins University Press.

Hua, F. (2009). Modeling, analysis and simulation of the Stokes-Darcy system with Beavers-Joseph interface condition (Doctoral Dissertation). Florida State University, Tallahassee, Florida.

Huntoon, P.W. (1995). Is it appropriate to apply porous media groundwater circulation models to karstic aquifers? In El-Kadi, A.I. (Ed.), *Groundwater models for resources analysis and management (pp.339-357).* Boca Raton, FL: Lewis Publishers.

Jeannin, P. (2001). Modeling flow in phreatic and epiphreatic karst conduits in the Holloch Cave (Muotatal, Switzerland). *Water Resources Research, 37*(2), 191-200.

Kincaid, T. R. (1999). *Morphologic and fractal characterization of saturated karstic caves*(Doctoral Dissertation). University of Wyoming, Laramie, Wyoming.

Kuniansky, E., Halford, K., & Shoemaker, W. (2008). Permeameter data verify new turbulence process for MODFLOW. *Ground Water, 46*(5), 768-771.

Liedl, R., Sauter, M., Huckinghaus, D., Clemens, T., & Teutsch, G. (2003). Simulation of the development of karst aquifers using a coupled continuum pipe flow model. *Water Resources Research, 39*(3)

Martin, J., & Dean, R. (2001). Exchange of water between conduits and matrix in the Floridan aquifer. *Chemical Geology, 179*(1-4), 145-165.

Marshak, S. (2008). *Earth: Portrait of a Planet* (3rd ed.). New York, N.Y.: Norton & Company Inc.

Mohrlok, U. (1996). Parameter-identifikation in doppel-kontinuum-modellen am beispiel von karst-aquiferen: Tubingen, Germany, Reihe C. Institut und Museum fur Geologie und Palaontologie der Universitat Tubingen, Tubinger Geowissenschaftliche Arbeiten, v. 31.

Palmer, A. (1991). Origin and morphology of limestone caves. *Geological Society of America Bulletin, 103*(1), 1-21.

Plummer, L., & Wigley, T. (1976). Dissolution of calcite in CO2 saturated solutions at 25 degrees C and 1 Atmosphere total pressure. *Geochimica Et Cosmochimica Acta, 40*(2), 191-202.

Plummer, L., Wigley, T., & Parkhurst, D. (1978). Kinetics of calcite dissolution in CO2 water systems at 5 degrees C to 60 degrees C and 0.0 to 1.0 ATM CO2. *American Journal of Science, 278*(2), 179-216.

Rose, H. E. (1945a). An Investigation into the Laws of Flow of Fluids through Beds of Granular Materials. *Proceedings of the Institute of Mechanical Engineers , 153*, 141-148.

Rose, H. (1945b). On the resistance coefficient - Reynolds number relationship for fluid flow through a bed of granular materials. *Proceedings of the Institute of Mechanical Engineers, 153*, 154-168.

Sauter, M. (1993). Double porosity models in karstified limestone aquifers – field validation and data provision. *Hydrogeological processes in karst terranes (Proceedings of the Antalya Symposium and Field Seminar, October 1990), IAHS Publication 207*, 261-279.

Scanlon, B., Mace, R., Barrett, M., & Smith, B. (2003). Can we simulate regional groundwater flow in a karst system using equivalent porous media models? Case study, Barton Springs Edwards aquifer, USA. *Journal of Hydrology, 276*(1-4), 137-158.

Shoemaker, W. B., Kuniansky, E. L., Birk, S., Bauer, S., & and Swain, E. D. (2007). *Documentation of a conduit flow process (CFP) for MODFLOW-2005 [electronic resource]:* U.S. Geological Survey Techniques and Methods, Book 6, Chapter A24, 50 p.

Shoemaker, W., Cunningham, K., Kuniansky, E., & Dixon, J. (2008). Effects of turbulence on hydraulic heads and parameter sensitivities in preferential groundwater flow layers. *Water Resources Research, 44*(3)

Spiessl, S., Prommer, H., Licha, T., Sauter, M., & Zheng, C. (2007). A process-based reactive hybrid transport model for coupled discrete conduit-continuum systems. *Journal of Hydrology, 347*(1-2), 23-34.

Thrailkill, J. (1974). Pipe flow models of a Kentucky limestone aquifer. *Groundwater, 12*(4), 202-205.

Teutsch, G. (1993). An extended double-porosity concept as a practical modeling approach for a karstified terrain. *Hydrogeological processes in karst terranes, (Proceedings of the Antalya Symposium and Field Seminar, October 1990), IAHS Publication 207*, 281-292.

Teutsch, G., & Sauter, M. (1998). Distributed parameter modelling approaches in karst hydrological investigations. *Bulletin d'Hydrogeologie 16*, 99-109.

Turnipseed, D.P., & Sauer, V.B. (2010). Discharge measurements at gaging stations: U.S. Geological Survey Techniques and Methods book 3, chap. A8, 87 p. (Also available at *http://pubs.usgs.gov/tm/tm3-a8/*.)

White, W.B. (1977). Role of solution kinetics in the development of karst aquifers. In Tolson, J.S. & Doyle, F.L. (Eds.), *Karst Hydrogeology: Congress of the International Association of Hydrogeologists*, 12^{th}, Memoirs, pp. 503 – 517.

White, W. B. (1988). *Geomorphology and hydrology of karst terrains*. New York: Oxford University Press.

White, W. B. (2002). Karst hydrology: Recent developments and open questions. *Engineering Geology, 65*(2-3), 85-105.

Yusun, C., & Ji, Bian. (1988). The media and movement of karst water. In Daoxian, Yuan (Ed.), *Karst Hydrogeology and Karst Environment Protection - Proceedings of the 21^{st} Congress of the International Association of Hydrogeologists in Guilin China, 10-15 October 198: Publication No. 176, Vol. 2* (pp. 555-564). Wallingford, Oxfordshire, UK: IAHS Press, Institute of Hydrology.

Zheng, C., & Wang, P.P. (1999). *MT3DMS: a modular three-dimensional multispecies model for simulation of advection, dispersion and chemical reactions of contaminants in groundwater systems.* Documentation and User's Guide, Contract Report SERDP-99-1, U.S. Army Engineer Research and Development Center, Vicksburg, MS (available at http://hydro.geo.ua.edu/).

BIOGRAPHICAL SKETCH

Josue Gallegos was born and raised in El Paso, Texas. He moved to Austin, Texas to pursue a degree in music composition at the University of Texas at Austin. However, an introductory geology course ignited his passion for science and geology, leading him to change majors and gain a Geology Bachelor of Science Degree in 2006. After working as a geologist for two years in Austin, Texas, Josue became specifically interested in Hydrogeology, and moved to Tallahassee, Florida to study Hydrogeology at Florida State University. He completed his research and graduated from Florida State University in 2011, with a Master of Science Degree in Geology.